scientific reports

Check for updates

OPEN

Structural and energetic basis of marine phytochemicals as dengue NS1 protein inhibitors

Sanjida Mahjabin Sanju[1,2,8], Md. Meherajul Kabir[1,3,8], Md. Ifteker Hossain[1,4], Ahamad Arafat Rizbi[1,5], Mehajabin Nusrat Nadia[1,4], Jannatul Ferdous[1,4], Mst. Ruma Akter[1,6], Nazia Kamal[1,7], Farhana Mansoor Priya[1,4] & Noimul Hasan Siddiquee[1,4]✉

Dengue, spread by *Aedes aegypti* and *Aedes albopictus*, causes 390 million infections, 50 million illnesses, and 24,000 fatalities, including over 4.5 million in 2023. This work finds DENV NS1 protein anti-virals beyond CYD-TDV using in silico approaches. Virtual screening and molecular docking were used to evaluate binding affinities, followed by toxicity profiling to assess pharmacokinetics and safety. Molecular dynamics simulations (200 ns) and MM-GBSA calculations measured the stability and binding strength of the protein-ligand complexes. Additionally, HOMO-LUMO analysis was performed to predict electronic properties and chemical reactivity. Based on natural availability and clinical relevance, 1,191 seaweed metabolite compounds were evaluated for therapeutic application. Due to their strong binding affinities (−5.567, −4.776, and − 4.550 kcal/mol), excellent ADME profiles, and low toxicity, CIDs 359, 8768, and 11,500,585 were screened out. Molecular docking showed hydrophobic interactions with ILE93 and ILE218, suggesting a pocket-wide active site for each ligand. After docking, MM-GBSA demonstrated negative binding free energies, HOMO-LUMO gaps, RMSD, RMSF, Rg, SASA, and hydrogen bonds were measured in MD simulations to confirm the protein-ligand complex's stability. CID 11,500,585 excelled in cumulative protein RMSD, RMSF, and SASA. After the simulation, MM-GBSA analysis confirmed their stability, with CID 11,500,585 (3,4-dibromo-5-(2-hydroxyethyl) benzene-1,2-diol) from *Rhodomela confervoides* seaweed having the lowest value of -25.18 kcal/mol at 200 ns. It may suppress DENV proliferation. QSAR study suggested that this chemical is anti-viral, although in vivo and in vitro testing is needed.

Keywords Dengue virus (DENV-NS1), Molecular dynamic simulation, Post simulation MM-GBSA, *Rhodomela confervoides* seaweed, 3,4-dibromo-5-(2-hydroxyethyl) benzene-1,2-diol

Dengue virus (DENV), the most common mosquito-borne flavivirus classified in the Flaviviridae family, is a major cause of illness and death, threatening individuals in tropical and subtropical regions. It is primarily transmitted by *Aedes aegypti* and, to a lesser extent, *Aedes albopictus*[1–3]. Human infections can result from any one of five serologically related but genetically distinct virus serotypes. According to epidemiological modelling, roughly 390 million people are infected with DENV annually, resulting in 50 million or more illnesses and 24,000 fatalities globally[4,5]. At present, DENV infection is prevalent in regions including the Americas, the Eastern Mediterranean, Southeast Asia, Africa, and the Western Pacific[6]. In the first ten months of 2023, there have been more than 4.5 million reported cases and over 4,000 deaths related to dengue across 80 countries and territories globally[7–9]. Serious syndromes such as dengue hemorrhagic fever or dengue shock syndrome can develop in rare cases after a dengue infection, while most cases are either asymptomatic or cause flu-like symptoms, including fever and rash[4,10,11].

DENV has a single-stranded RNA genome that is about 10,700 bases long. The genome is surrounded by a capsid protein, a lipid membrane derived from the host, and embedded with glycoproteins and membrane proteins[7,12]. Following capsid protein uncoating from the nucleocapsid, genomic RNA translates seven non-

[1]Bioinformatics Laboratory (BioLab), Noakhali 3814, Bangladesh. [2]Department of Zoology, Feni Govt. College, Feni 3900, Bangladesh. [3]Department of Pharmacy, International Islamic University Chittagong, Chittagong 4318, Bangladesh. [4]Department of Microbiology, Noakhali Science and Technology University, Noakhali 3814, Noakhali, Bangladesh. [5]Department of Applied Chemistry and Chemical Engineering, Noakhali Science and Technology University, Noakhali 3814, Noakhali, Bangladesh. [6]Department of Microbiology, Gono Bishwabidyalay, Savar, Dhaka 1344, Bangladesh. [7]Pioneer Dental College, Dhaka 1229, Bangladesh. [8]Sanjida Mahjabin Sanju and Md. Meherajul Kabir have contributed equally to this work. ✉email: noimul.microbiology.nstu@gmail.com

structural proteins (NS1, NS2A, NS2B, NS3, NS4A, NS4B, and NS5) and three structural proteins, the membrane precursor protein, the capsid protein, and the envelope protein[11,13–15]. Among the non-structural proteins produced by the dengue virus, NS1 has gained significant attention as a potential therapeutic target due to its crucial role in immune evasion and viral replication[13,16]. While structural proteins mostly help viral entry and assembly, NS1 serves dual functions: it promotes replication inside the host cell and leads to immunopathogenesis outside the cell[17,18]. These functions underscore its central role in dengue disease progression; thus, NS1 has become a major focus for developing antiviral drugs.

The NS1 is a promising target since it is crucial for the life cycle and pathogenesis of the dengue virus. Compared to other flaviviruses, NS1 is a 48-kDa conserved N-linked glycoprotein that the host cell synthesizes as a monomer and subsequently dimerizes following post-translational modification in the endoplasmic reticulum lumen[15,19–21]. In immune system evasion, NS1 functions as a secreted hexamer[22]. NS1 performs multifunctional roles: intracellular NS1 facilitates viral replication and assembly, while the secreted form exits infected cells, circulates in the host's system, and assists in immune evasion[4,23,24]. By disrupting this function, DENV inhibits. NS1 activates macrophages, platelets, and mononuclear peripheral cells via binding to Toll-like receptor 4 (TLR4). Immune cell activation triggers the production of a cascade of pro-inflammatory cytokines, which disrupt cellular tight junctions[25–27]. Still, NS1 plays a crucial role in infected cells because it spatially coincides with the double-stranded RNA replicative form, thus acting as an essential cofactor in the viral RNA replication process[5,11,28]. NS1 dimers and sNS1 hexamers that are also linked to the cell surface have a strong immunogenic effect[29]. These dual functions in external immune disruption and intracellular replication highlight NS1's crucial role in the progression of dengue disease, thereby guiding attention for drug research and vaccine design[30,31].

Until now, no specific treatment has been found for dengue other than supportive measures and fluid therapy[32]. Acetaminophen (paracetamol) is used to control pain, and non-steroidal anti-inflammatory drugs like ibuprofen are avoided to prevent the risk of bleeding[33]. However, acetaminophen is associated with hepatotoxicity and elevated liver enzymes, which is particularly risky in dengue-induced liver stress, and overdose can cause acute liver failure[34,35]. Although infection provides temporary protection against one serotype, it cannot help in the case of other serotypes[36]. Therefore, there is an ongoing need for improved vaccine development. Vaccine development has advanced, highlighted by the licensing of the Chimeric Yellow Fever Dengue Tetravalent Vaccine (CYD-TDV), commercially known as Dengvaxia, by Sanofi Pasteur, which has been utilised in Southeast Asia and Latin America[28,37]. However, CYD-TDV increases the risk of severe dengue in seronegative individuals due to antibody-dependent enhancement (ADE), limiting its use only to those with prior dengue exposure[38,39]. At the same time, TAK-003 (QDENGA) by Takeda Pharmaceuticals shows promising efficacy and is deployed in Europe, Indonesia, and Brazil[40,41]. Although TAK-003 demonstrates strong protection, it has reported side effects such as fever, injection site pain, and rare anaphylaxis; it is also not yet approved for use in the USA[42,43]. TV005, developed by NIH, is a promising dengue vaccine undergoing clinical trials for protection against all four serotypes[44,45]. TV005 has shown mild side effects like rash and transient neutropenia during trials and remains unapproved as it is still under clinical development[46].

Recent studies have identified promising antiviral compounds derived from marine organisms, including Gymnochrome D and Isogymnochrome D, isolated from *Gymnocrinus richeri*[47]along with Scequinadoline A from *Dichotomomyces cejpii* F31- 1, have demonstrated potent in vitro antiviral activity against dengue virus, underscoring their therapeutic potential[48]. However, despite these promising results, no in-silico studies have been conducted to explore the antiviral potential of seaweed-derived metabolite compounds targeting the NS1 protein, representing a major gap in current research. The potential of seaweed metabolites as antiviral agents is well-documented, with numerous reports highlighting their antioxidant, antiviral, antimicrobial, and anti-inflammatory properties[49,50]. Given their accessibility and environmental sustainability, seaweed-derived compounds hold promise for developing safe, effective antiviral treatments[51,52]. For this specific objective, this study focused on seaweed metabolite compounds.

This study aims to address this gap by employing Computer-Aided Drug Design (CADD) methods to identify and evaluate seaweed metabolites that may inhibit the NS1 protein of DENV, by utilizing techniques such as binding affinity analysis, pharmacokinetics (PK), and toxicological profile analysis, MM-GBSA analysis, quantum mechanical (QM) calculation, HOMO-LUMO, QSAR, and molecular dynamics (MD) simulations that represent a step forward in leveraging marine-derived compounds for dengue therapy.

Moreover, various advanced in silico methodologies have significant potential to augment the depth and precision of computational studies. Methods such as Molecular Mechanics Poisson–Boltzmann Surface Area (MM-PBSA) computations, steered molecular dynamics (SMD), and umbrella sampling simulations can substantially enhance the accuracy of binding free energy assessments and mechanistic understanding[53,54]. Furthermore, analyses including desolvation energy, buried surface area, restraint violation energy, ATP-binding cavity profiling, complementarity evaluations, and distance and density plot assessments reflect advanced methodologies that could significantly enhance the depth and predictive capability of the study[55–57].

Results

Molecular Docking analysis

Molecular docking was conducted utilizing the target protein and 1191 seaweed metabolite compounds. Out of these compounds, the top six compounds having the highest binding affinity are CID 359 (BE001), CID 8768 (RP004), CID 180,306 (GA011), CID 237,332 (RL333), CID 5,352,074 (RL462), and CID 11,500,585 (RR059) exhibiting docking scores of −5.567, −4.776, −4.622, −4.581, −4.567, and − 4.55 kcal/mol, respectively, which were chosen for further study (Fig. 1), and their sources along with their therapeutic uses are mentioned in Table 1.

The compounds that were identified indicated strong binding affinities for conserved amino acid residues within the NS1 binding region. CID 359 exhibits interactions with ILE93, ILE218, and MET97, whereas CID

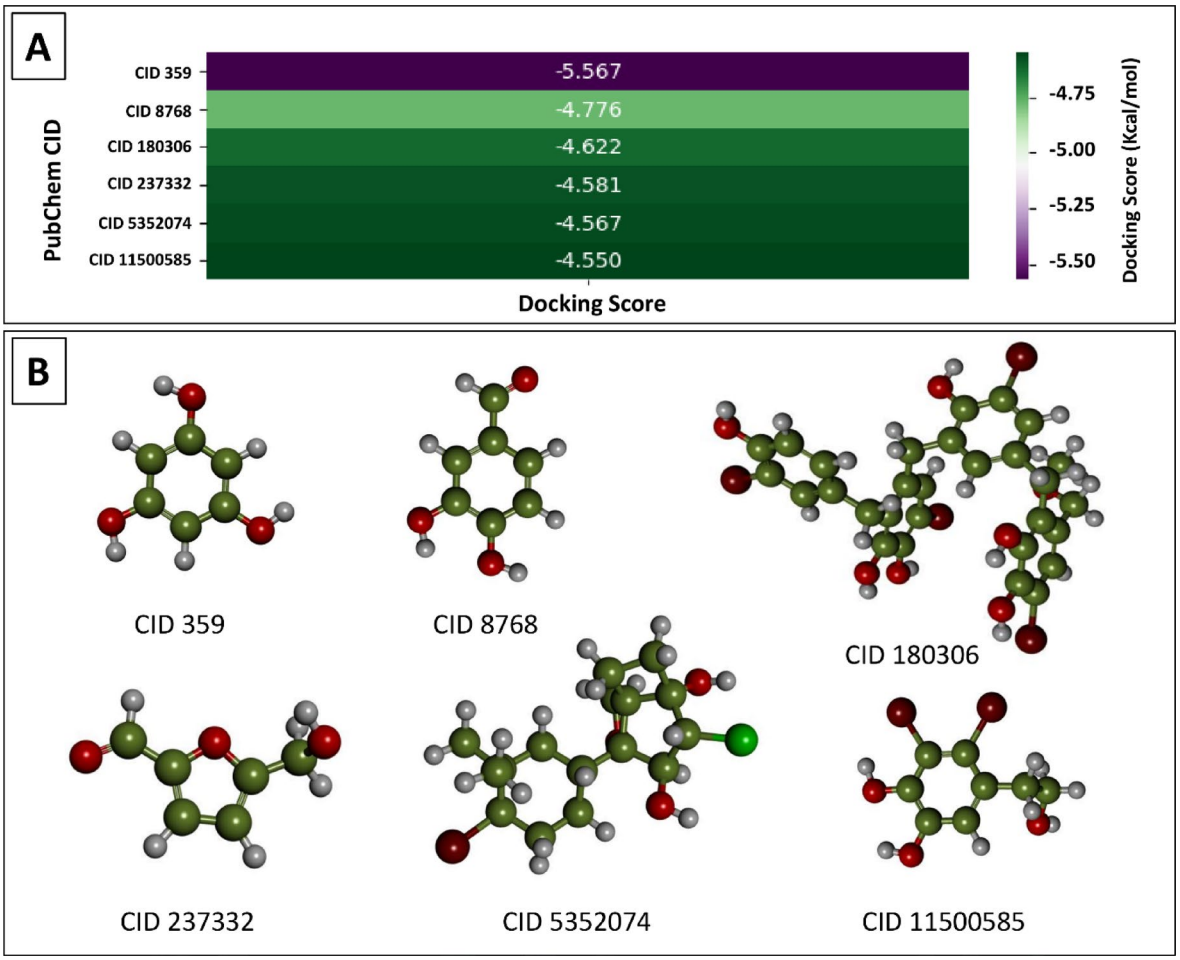

Fig. 1. Molecular docking heat map visualisation diagram for binding energy (**A**) and compound identification using three-dimensional (3D) configuration (**B**).

PubChem CID	Compound name	Source	Geographical origin	Therapeutic use
359	Phloroglucinol	*Ecklonia stononifera*	Gijang-gun, Busan	Analgesic and Antispasmodic [122], Antiviral, Anti-bacterial, Anti-oxidant, Anti-Inflammatory, Anti- cancer [123]
8768	Protocatechualdehyde	*Polysiphonia lanosa*	Kimmeridge Bay, Dorset, England	Anti-EMT & Anti-fibrosis [124]
180,306	Rawsonol	*Avrainvillea rawsonii*	Baby Beach, Aruba, Netherlands Antilles	Hypocholesterolemic effect [125]
237,332	5-hydroxymethyl-2-furfural	*Laurencia undulata*	Cheju Island, South Korea	Anti-sickling [126], Anti-hypoxic effect [127]
5,352,074	Majapol A	*Laurencia majuscula*	Apo island, Negros Island, Central Visayas, Philippines	Cytotoxicity [128]
11,500,585	3,4-dibromo-5-(2-hydroxyethyl)benzene-1,2-diol	*Rhodomela confervoids*	Dalian, Liaoning Province, Republic of China	Antioxidant activity [129]

Table 1. Compounds are identified according to pubchem CID, as well as the name, source, and geographical origin of the top six compounds, including their therapeutic uses.

8768 engages with ILE93 and ILE218. CID 11,500,585 demonstrates a wider interaction profile involving GLY95, LEU270, ILE93, ILE218, VAL220, and MET97. All of these amino acids are conserved within the binding area, highlighting their potential importance in enhancing the stability and specificity of ligand binding.

Pharmacokinetics profiling and toxicity properties analysis

In this study, the ADME characteristics and toxicity profiles of the six highest docking score compounds were analyzed to evaluate their potential impact on the body. These six compounds are CIDs 359, 8768, 180,306, 237,332, 5,352,074, and 11,500,585, respectively. The initial analysis revealed that CIDs 359 and 8768 comply

with Lipinski's rule and exhibit low toxicity, making them suitable candidates for further investigation. Previous studies have demonstrated that compounds with modest toxicity can be approved as drugs based on necessity[58,59]. The compound, CID 180,306, violated Lipinski's rule due to its high molecular weight of 804.11 g/mol, which may limit its drug-like potential. In contrast, the fourth and fifth compounds (CID 237332 and 5352074) have no Lipinski violations; however, their unfavorable toxicity profiles rendered them unsuitable as drug candidates (shown in Supplementary 1). The sixth compound exhibited no Lipinski violations and demonstrated a lower toxicity profile. Hence, the three compounds' CIDs 359, 8768, and 11,500,585 showed the most promising results and were selected for further optimization to aid in developing novel drugs, as presented in Figs. 2 and 3.

Analysis of Protein-Ligand interaction

The selected lead compounds interacted with the target protein and shared amino acid (AA) residues during the molecular docking phase. CID 359 and CID 8768 commonly formed H-bonds with ILE93 and ILE218, while CID 11,500,585 formed H-bonds with GLY95 and LEU270. All three compounds contain ILE93 and ILE218 AA residues, which form hydrophobic bonds, indicating that they bind to the same binding pocket of the protein. In this binding, CIDs 359, 8768, and 11,500,585 are represented by green, blue, and pink, respectively, as shown in Fig. 4A. These findings are comprehensively documented in Table 2 and illustrated in Fig. 4.

Post-docking MM-GBSA analysis

The lead compounds' binding free energies (ΔG Bind) (CIDs 359, 8768, and 11500585) with the target protein have been calculated using MM-GBSA calculations. The findings demonstrated that each of the three molecules displayed the lowest binding free energies, measuring − 20.50, −24.9, and − 27.7 kcal/mol, respectively. Among them, CID 8768 and CID 11,500,585 exhibited the lowest binding free energy relative to CID 359, indicating their potential to sustain prolonged interaction with the target protein and efficiently inhibit its function, as illustrated in Fig. 5 and Supplementary 2.

Quantum mechanical (QM) calculation

The leads CIDs 359, 8768, and 11,500,585 demonstrated a HOMO-LUMO energy values of (−0.23326 a.u. or −6.34731 eV and − 0.00394 a.u. or −0.10721 eV), (−0.23380 a.u or −6.362007 eV and − 0.07087 a.u or −1.928466 eV) and (−0.22450 a.u or −6.1089423 eV and − 0.03464 a.u. or −0.9426002 eV), respectively, in atomic mass units and Electro Volt (eV) shown in Table 3; Fig. 6. The green and red colors signify the positive and negative phases, respectively. HOMO-LUMO gap, Hardness, and Softness scores of leads were calculated, and the results were (6.2401009, 4.43354, and 5.16634) eV, (3.120050, 2.216770, and 2.583177) eV, and (0.160253, 0.225553, and 0.19356) eV, respectively. A larger HOMO-LUMO energy gap signifies greater stability and higher chemical hardness than a smaller gap[60]. The lead compounds exhibit stability and chemical reactivity in the order CID 8768 > CID 11,500,585 > CID 359. While all of them are promising candidates for drug design, CID 8768 and CID 11,500,585 demonstrate greater stability due to their HOMO-LUMO gap values, making them more favorable for possible drug candidates.

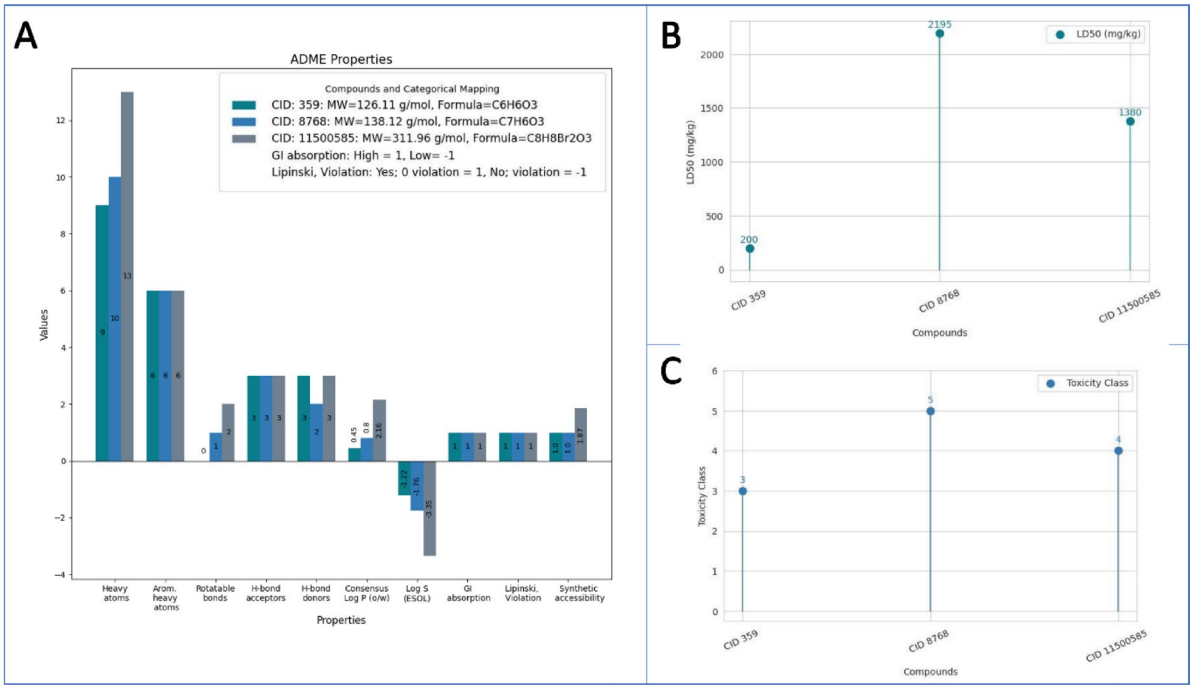

Fig. 2. ADME properties (**A**), predicted LD50 values (**B**), and corresponding toxicity classes (**C**) for lead compounds CID 359, CID 8768, and CID 11500585.

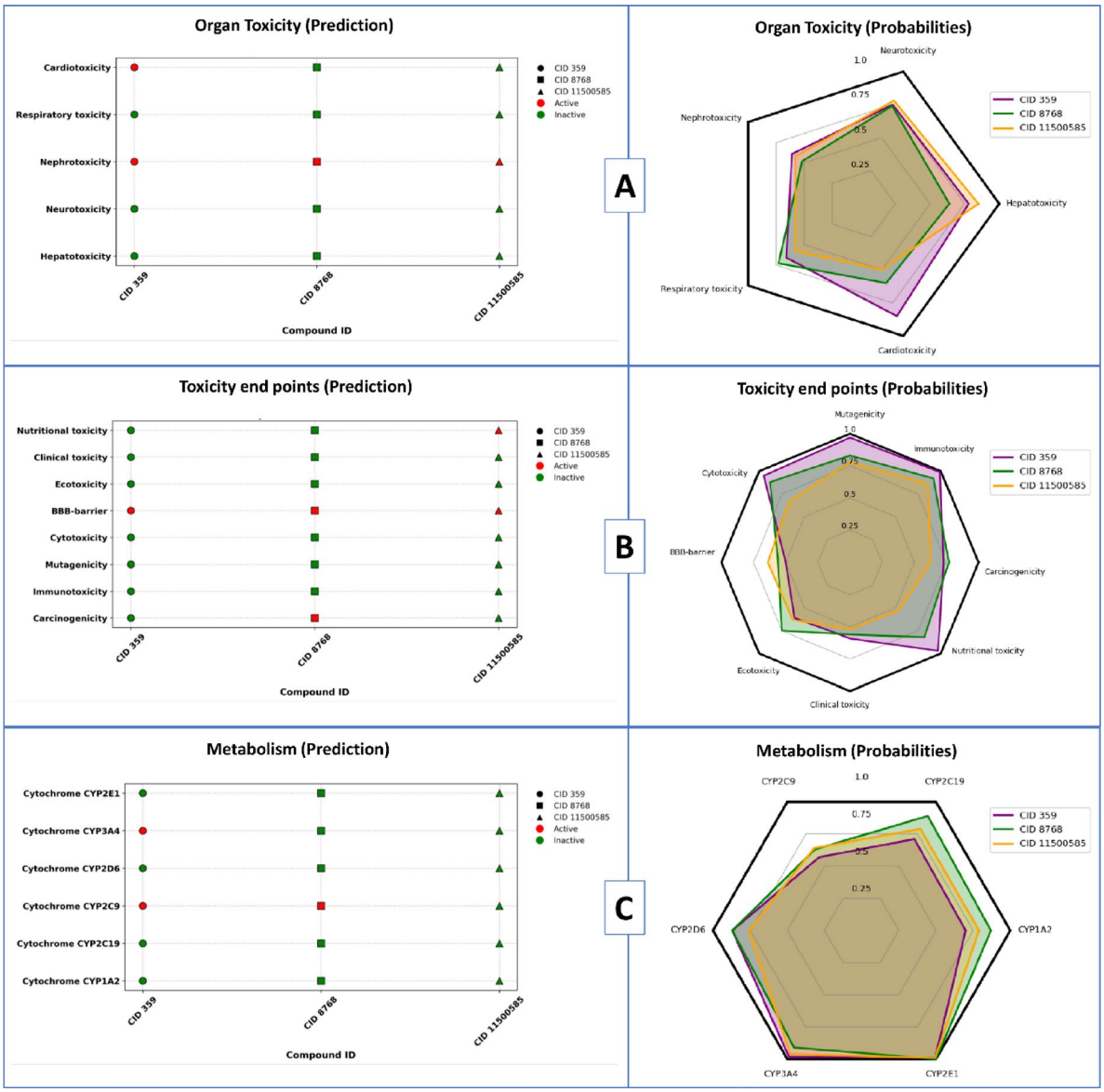

Fig. 3. Graphical representation of the toxicity assessment of lead compounds. Organ toxicity (**A**), Toxicity end points (**B**), and Metabolism (**C**). Each parameter includes toxicity prediction (left) and corresponding probability values (right).

QSAR analysis

QSAR analysis using the online PASS program was conducted to analyze the chemical properties of the chosen compounds and assess their potential for biological activity before the MD simulation, and Table 4 presents the outcomes of the QSAR models. CID 359 exhibits activity as a membrane integrity agonist (MIA), JAK2 expression inhibitor, thioredoxin inhibitor, membrane permeability inhibitor (MPI), and Pin1 inhibitor, all of which may directly influence pathways involved in viral entry, replication, and immune modulation. Whereas, CID 8768 also possesses an MIA, MMP9 expression inhibitor, a thioredoxin inhibitor, and MPI, which are the activities that may more directly inhibit the dengue virus by impacting its entry, replication, or spread. Lastly, CID 11,500,585 shows biological behavior like JAK2 expression inhibitor, Antiviral (Adenovirus, CMV, Herpes), HIV-1 integrase (Overall Integration) inhibitor, RNA-directed DNA polymerase inhibitor, HIV-1 integrase (Strand Transfer) inhibitor activity. These activities target viral replication and infection mechanisms, which may also be relevant for dengue virus inhibition.

MD simulation analysis

During the 200 ns MD simulation, which generated 1000 frames with a 200 ps interval for trajectory recording and analyzed the trajectory file to evaluate protein and ligand Root Mean Square Deviation (RMSD), Root Mean Square Fluctuation (RMSF), Solvent-Accessible Surface Area (SASA), Radius of gyration (Rg), and protein-

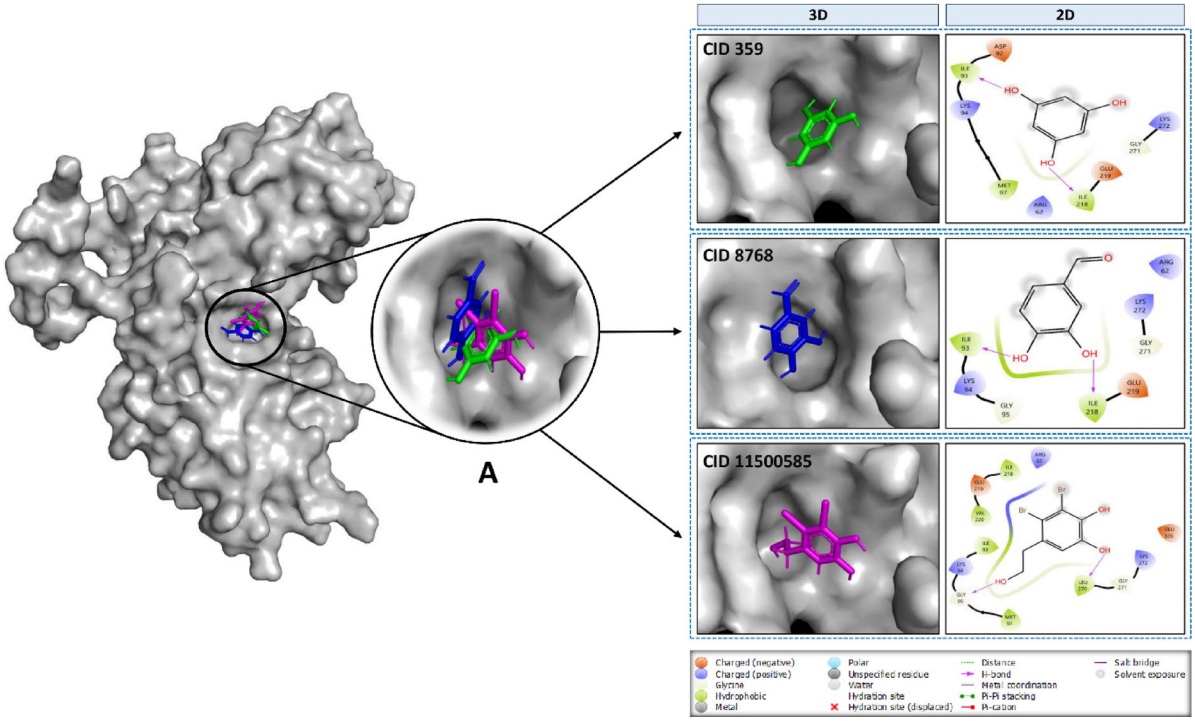

Fig. 4. Interaction between the NS1 protein and the ligands, where **A** represents the ligand complex, the same active pocket of the protein, and CID 359, CID 8768, and CID 11500585 are illustrated in both 3D and 2D formats.

CID	Compound name	H-Bond	Hydrophobic bond
359	Phloroglucinol	ILE93, ILE218	ILE93, ILE218, MET97
8768	Protocatechualdehyde	ILE93, ILE218	ILE93, ILE218
11,500,585	3,4-dibromo-5-(2-hydroxyethyl) benzene-1,2-diol	GLY95, LEU270	ILE93, ILE218, VAL220, MET97, LEU270

Table 2. Demonstrated the amino acid residues during the formation of H-bonds and hydrophobic bonds between the selected three compounds and the targeted protein.

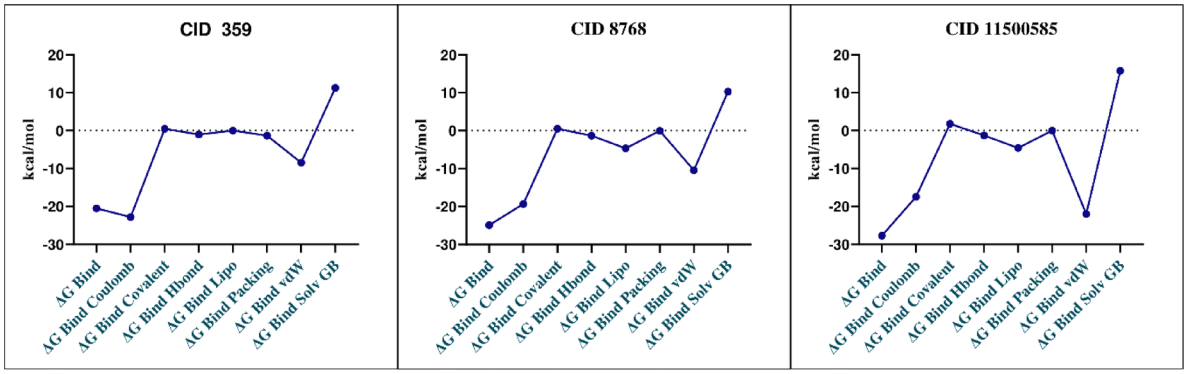

Fig. 5. Post-docking MM-GBSA ΔG_bind values for lead compounds CID 359, CID 8768, and CID 11500585, indicating their predicted binding affinities.

ligand contact utilizing the Simulation Interaction Diagram (SID), as shown in Fig. 7. Hydrogen bonds between atom subsets, as well as intermolecular hydrogen bonds between the ligand and the protein, were analyzed.

CID	HOMO (eV)	LUMO (eV)	HOMO-LUMO Gap (eV)	Hardness (eV)	Softness (eV)
359	−6.34731	−0.10721	6.2401009	3.12005	0.160253
8768	−6.362007	−1.928466	4.43354	2.21677	0.225553
11,500,585	−6.1089423	−0.9426002	5.16634	2.583177	0.19356

Table 3. Results of DFT calculations of the lead compounds HOMO-LUMO analysis are below.

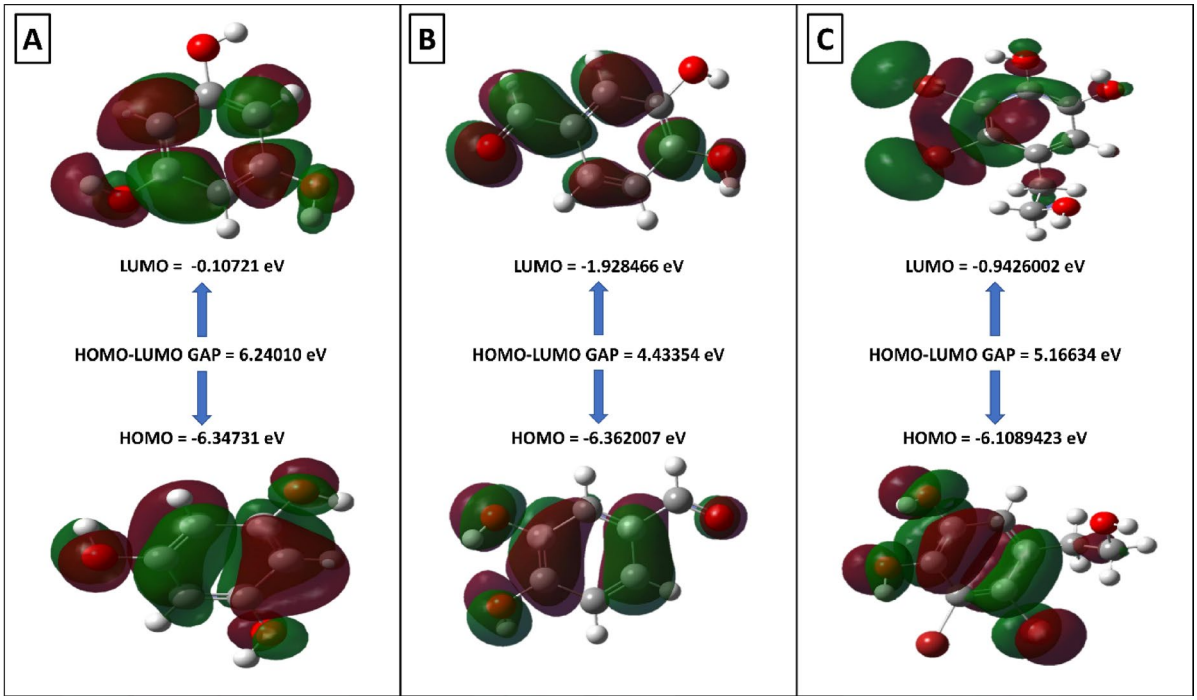

Fig. 6. Three-dimensional (**3D**) representations of the lead compounds: (**A**) CID 359, (**B**) CID 8768, and (**C**) CID 11500585, including their associated HOMO (Highest Occupied Molecular Orbital) and LUMO (Lowest Unoccupied Molecular Orbital) energy values.

Protein RMSD analysis

RMSD in MD simulation calculates the average displacement of a chosen atom relative to a reference point, and is used to evaluate structural changes in proteins for the three lead compounds, while also assessing system equilibration for stability and reliability[61,62]. Blue, orange, grey, and yellow represent the protein RMSD values for the apoprotein and lead compounds CID 359, 8768, and 11,500,585 (Fig. 7A). The lowest and highest RMSD values of apoprotein were 1.443 Å and 4.836 Å, which were observed at frame numbers 2 and 299, respectively. The lowest RMSD values of the leads CIDs 359, 8768, and 11,500,585 were 1.754 Å, 1.876 Å, and 1.235 Å, respectively, in frame numbers 1, and the highest were 5.05 Å, 27.283 Å, and 4.576 Å in frame numbers 304, 868, and 907, respectively. The differences between their highest and lowest RMSD values seem to be: 3.393 Å, 3.296 Å, 25.407 Å, and 3.341 Å, respectively. The average RMSD values of the apoprotein and leads (CIDs 359, 8768, and 11500585) were 4.094 Å ± 0.420, 4.368 Å ± 0.330, 7.135 Å ± 7.069, and 3.838 Å ± 0.408, respectively. The compound, CID 8768, showed much more fluctuation than apoprotein and the other two compounds. Therefore, the other two compounds (CIDs 359 and 11500585) were very close to the apoprotein throughout the simulation time and showed excellent RMSD results with no major fluctuation. Overall, the compound, CID 11,500,585, is very close to the native structure and becomes more stable after complexing with apoprotein, demonstrating outstanding stability, as its average RMSD value is 3.838 Å (Supplementary 3).

Ligand RMSD analysis

The ligand RMSD measures the average displacement of atomic positions between a ligand's present and reference conformations. A smaller score denotes stability; fluctuations point to instability[63]. Ligand RMSD values are derived from the complex structures' ligand atoms. Blue, gray, and orange represent the ligand RMSD values for the lead compounds, CIDs 359, 8768, and 11,500,585 (Fig. 7B). The average ligand RMSD values for leads CIDs 359, 8768, and 11,500,585 were 0.0885 Å ± 0.0123, 0.3787 Å ± 0.1661, and 0.6934 Å ± 0.1273, respectively. The highest and the lowest RMSD values of CID 359 are 0.126 Å and 0.05 Å; CID 8768 are 0.088 Å and 0.654 Å; CID 11,500,585 are 0.105 Å and 1.085 Å (Supplementary 4).

CID	Phytoconstituents	Pa	Pi	Biological activity
359	Phloroglucinol	0.941	0.004	Membrane integrity agonist
		0.938	0.004	HIF1A expression inhibitor
		0.934	0.003	Ubiquinol-cytochrome-c reductase inhibitor
		0.916	0.002	APOA1 expression enhancer
		0.885	0.004	JAK2 expression inhibitor
		0.884	0.003	Fatty-acyl-CoA synthase inhibitor
		0.856	0.003	Thioredoxin inhibitor
		0.857	0.005	Membrane permeability inhibitor
		0.826	0.004	Acetylesterase inhibitor
		0.817	0.008	Protein-disulfide reductase (glutathione) inhibitor
		0.788	0.003	N-acetylneuraminate synthase inhibitor
		0.742	0.005	MMP9 expression inhibitor
		0.736	0.003	Endo-1,3(4)-beta-glucanase inhibitor
		0.732	0.005	Pin1 inhibitor
		0.721	0.003	Estrogen antagonist
		0.712	0.002	Astringent
		0.702	0.005	Leucolysin inhibitor
		0.689	0.014	Lipoprotein lipase inhibitor
		0.668	0.006	Erythropoiesis stimulant
8768	Protocatechualdehyde	0.919	0.005	Aspulvinone dimethylallyltransferase inhibitor
		0.875	0.017	Membrane integrity agonist
		0.812	0.003	MMP9 expression inhibitor
		0.730	0.007	Thioredoxin inhibitor
		0.717	0.005	MAP kinase stimulant
		0.733	0.026	Membrane permeability inhibitor
		0.718	0.013	Apoptosis agonist
11,500,585	3,4-dibromo-5-(2-hydroxyethyl)benzene-1,2-diol	0.911	0.006	Aspulvinone dimethylallyltransferase inhibitor
		0.803	0.004	Antiseptic
		0.783	0.040	Membrane integrity agonist
		0.662	0.004	2,3-Dihydroxyindole 2,3-dioxygenase inhibitor
		0.680	0.034	Alkenylglycerophosphocholine hydrolase inhibitor
		0.663	0.032	Antineoplastic
		0.652	0.030	GST A substrate
		0.635	0.032	Glucose oxidase inhibitor
		0.619	0.009	Antimutagenic
		0.610	0.023	Peroxidase inhibitor
		0.600	0.003	Sickle-cell anemia treatment
		0.597	0.011	1-Alkylglycerophosphocholine O-acetyltransferase inhibitor
		0.572	0.023	Trimethylamine-oxide aldolase inhibitor
		0.573	0.037	JAK2 expression inhibitor
		0.501	0.069	Platelet aggregation stimulant
		0.515	0.106	Saccharopepsin inhibitor
		0.489	0.029	Chitinase inhibitor
		0.477	0.021	Laccase inhibitor
		0.389	0.034	Antiviral (Adenovirus)
		0.315	0.021	Antiviral (CMV)
		0.344	0.064	Antiviral (Herpes)
		0.247	0.007	HIV-1 integrase (Overall Integration) inhibitor
		0.256	0.047	RNA directed DNA polymerase inhibitor
		0.215	0.007	HIV-1 integrase (Strand Transfer) inhibitor
		0.287	0.098	Antiviral (Influenza)

Table 4. The findings from the QSAR models regarding the prediction of bioactivity for the chosen compounds. **Pa* (Probability of activity), *Pi* (probability of inactivity).

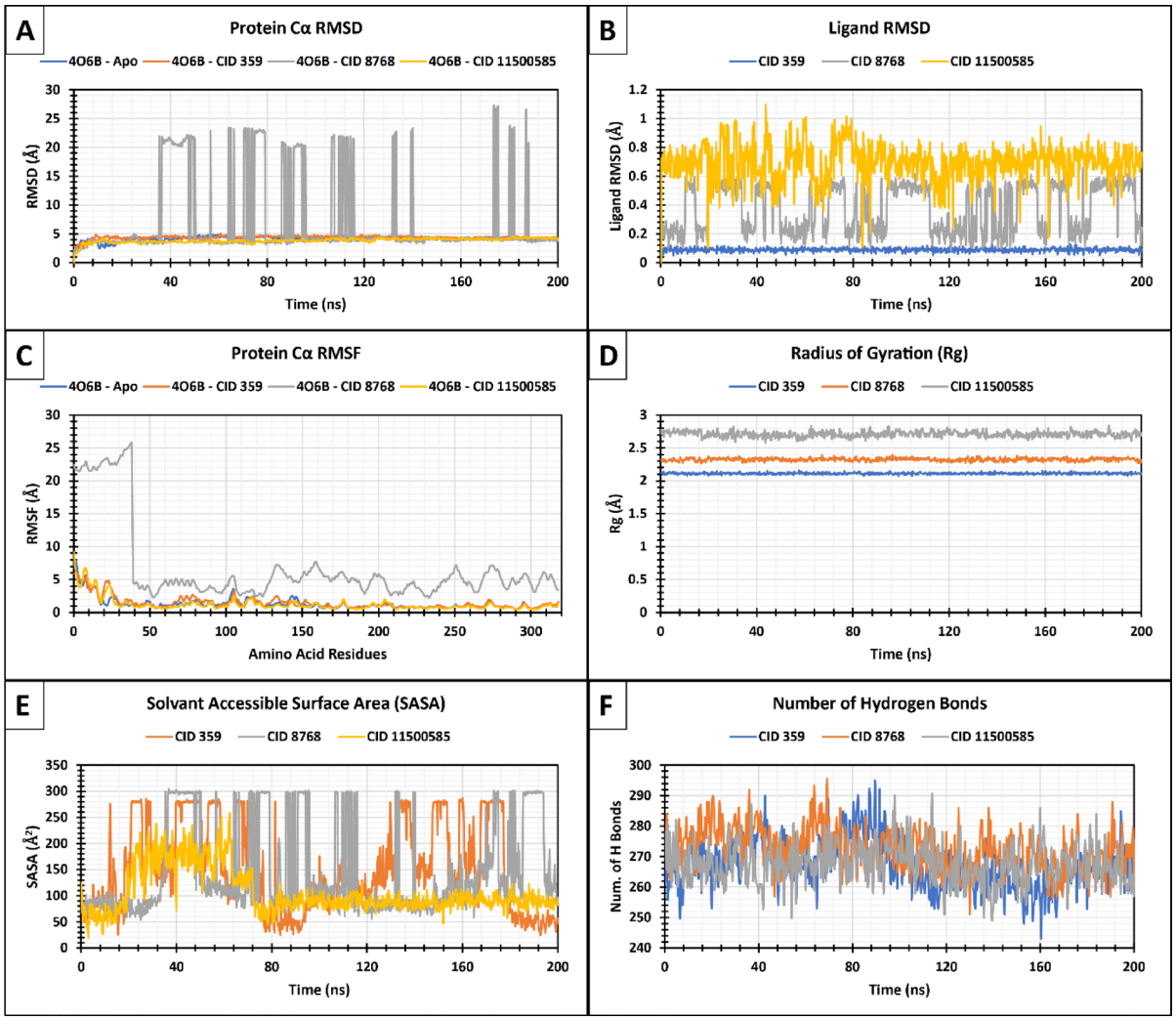

Fig. 7. The apoprotein's Protein RMSD (**A**), Ligand RMSD (**B**), RMSF (**C**), Rg (**D**), SASA (**E**), and Number of Hydrogen Bonds (**F**) data are illustrated as complexed with the three leads chosen and extracted from the 200 ns MD trajectory of the complex system's Cα atoms.

RMSF analysis

Root Mean Square Fluctuation (RMSF) serves as a tool to assess the local variations in the positions of protein chain residues and ligand atoms[61]. To evaluate protein structural flexibility upon ligand binding, RMSF values were calculated for the unbound apoprotein and the protein ligand complexes (CIDs 359, 8768, and 11500585); this analysis focused on localized structural variations at specific residue sites, offering insights into the dynamic behavior of the protein during ligand interaction (Fig. 7C). Apoprotein's RMSF values were observed to be lowest at LEU_321 and highest at ASP_1; the residual positions and the values were 0.445 Å and 7.951 Å, respectively, and the difference is 7.506 Å. Besides, the lead compounds, CIDs 359, 8768, and 11,500,585, having the lowest and highest RMSF values were like that: the lowest were 0.469 Å, 2.233 Å, and 0.459 Å, which were observed at LEU_321, ILE_264, and LEU_321 residual positions, respectively; the highest values were 5.944 Å, 25.741 Å, and 9.162 Å, observed at the ASP_1, LYS_41, and ALA_0 residual positions, respectively. The differences between their highest and lowest RMSF values seem to be 5.475 Å, 23.518 Å, and 8.703 Å, respectively. The average RMSF values of apoprotein and the lead compounds (CIDs 359, 8768, and 11500585) were, in that order, 1.329 Å ± 0.987, 1.468 Å ± 0.994, 6.763 Å ± 6.139, and 1.247 Å ± 1.100. Compared to the apoprotein, the compound CID 359 has nearly the same stability following complex formation, whereas CID 11,500,585 exhibits the highest stability following complex formation. However, the CID 8768 (average RMSF value of 6.763 Å) had excessive fluctuations during the simulation phase after making a complex with the protein. In summary, it has been observed that CID 11,500,585 has the lowest average RMSF value of 1.247 Å than the apoprotein, denoting the least fluctuations and most stability during the formation of a complex with the targeted protein in comparison to others (Supplementary 5).

Evaluation of the radius of gyration

The radius of gyration (Rg) of the protein-ligand complex was analyzed to determine protein mobility and stiffness, as it reflects changes in compactness and serves as a critical measure of macromolecular structural activity[62,64]. A low and stable Rg value generally signifies that the protein retains a compact conformation during the simulation, implying a stable and well-folded structure upon ligand binding. Conversely, higher or drastically variable Rg values might indicate conformational alterations induced by ligands, structural flexibility, or even partial unfolding, which could suggest a potential destabilisation of the complex[65,66].

The average Rg values for CID 359, CID 8768, and CID 11,500,585 were 2.112 Å ± 0.0129, 2.323 Å ± 0.0215, and 2.709 Å ± 0.0419, respectively (Fig. 7D). Compounds CIDs 359, 8768, and 11,500,585 showed a steadier range of variations, with minimum and maximum values of 2.068 Å in the 495 number frame to 2.157 Å in the 288 number frame (the difference is 0.089 Å), 2.262 Å in the 84 number frame to 2.396 Å in the 482 number frame (the difference is 0.134 Å) and 2.58 Å in the 218 number frame to 2.843 Å in the 932 number frame (the difference is 0.263 Å), respectively (Supplementary 4).

Solvent accessible surface area analysis

A vital part of MD simulations is solvent-accessible surface area (SASA) analysis, which helps to figure out how a drug and a protein interact in the most important ways. This method makes it easier to find the drug's binding site by looking at places where molecules are less easily accessible[67]. The SASA value indicates molecular compactness, where lower values denote a more compact structure and larger values imply a more open conformation[68]. The lowest SASA values of the selected leads CID 359, 8768, and 11,500,585 were 25.196 $Å^2$, 48.084 $Å^2$, and 19.307 $Å^2$, and were observed at frame numbers 964, 67, and 15, respectively (Fig. 7E). The highest values observed at frame numbers 800, 184, and 312 were 286.465 $Å^2$, 304.263 $Å^2$, and 257.942 $Å^2$, respectively. Differences in their highest and lowest values seem to be 261.269 $Å^2$, 256.179 $Å^2$, and 238.635 $Å^2$, respectively. Those selected compounds have average values of 154.021 $Å^2$ ± 85.06, 146.410 $Å^2$ ± 86.53, and 106.230 $Å^2$ ± 42.29. The assessed average SASA value for the complex system varied between 19 $Å^2$ and 305 $Å^2$, suggesting a notable level of accessibility of amino acid residues to the chosen chemicals within the complex systems. The average SASA value for CID 11,500,585 is lower than others, which means it is more deeply ingrained in the complex system's protein binding pocket. This makes it better able to change the biological activity of the target than other compounds (Supplementary 4).

Analysis of hydrogen bonds between atom subsets and Protein-Ligand contacts analysis

Hydrogen bonds are crucial for drug properties like selectivity, absorption, and metabolism. They facilitate interactions between ligands and their unique protein binding sites[69]. A 200-ns simulation run monitored H-bond formation between atoms and the substance (Fig. 7F). All compounds generated multiple H-bonds, ranging from 243 to 295. The highest number of H-bonds for CIDs 359, 8768, and 11,500,585 were 295, 295, and 290, respectively. The average H-bond numbers for CID 359, CID 8768, and CID 11,500,585 were 266, 268, and 265, respectively (Supplementary 4). Analyzing these bonds provides insights into a drug's properties.

Protein-ligand (P-L) contacts analysis has been completed through SID over a 200 ns simulation period, which analyzed the intermolecular connections between lead compounds (CIDs 359, 8768, and 11500585) and their targeted protein. P-L contacts have been assessed using hydrogen bonds, ionic bonds, non-covalent bonds (hydrophobic bonds), and water bridges. CID 359 generated multiple interactions (more than two) at the residues PRO_36, HIS_50, CYS_55, LEU_66, HIS_77, SER_80, GLU_83, VAL_84, ILE_93, LYS_94, LYS_101, ARG_102, HIS_129, LEU_134, PRO_138, CYS_143, GLN_175, LYS_272 (Fig. 8A). Multiple interactions with CID 8768 were generated by residues LYS_94 (0.07), ILE_96 (0.03), PRO_106 (0.04), HIS_269 (0.06), LYS_272 (0.05), GLU_274 (0.02) (Fig. 8B), while multiple interactions were made by CID 11,500,585 at the residues ARG_62 (0.17), LYS_69 (0.1), ASP_92 (0.16), ILE_93 (0.76), LYS_272 (0.12), correspondingly (Fig. 8C). However, the molecule CID 359 interacts with apoprotein through strong hydrogen and various bond interactions with the apoprotein, indicating a possibility of more stable and effective binding.

CID 359 and CID 8768 had more interactions overall, although their interaction fraction values were comparatively lower. But both compounds had good interaction fractions with some specific amino acids. For example, CID 359 interacted well with PHE_34, CYS_55, and LEU_134, and CID 8768 interacted well with ILE_218, GLU_326, and ASP_327. CID 11,500,585, on the other hand, had fewer contacts overall but had a good number of hydrogen bonds, hydrophobic interactions, ionic bonds, and water bridges, all of which had high interaction fraction values.

Analysis of intermolecular hydrogen bonds between the ligand and the protein

The intermolecular hydrogen bonds formed between the ligands and the target protein were analyzed throughout the 200 ns molecular dynamics (MD) simulation period (Fig. 9). The complex formed between CID 359 and the target protein exhibited a maximum of 4 intermolecular hydrogen bonds at frame 425, with an average of 0.824 hydrogen bonds throughout the simulation. For the CID 8768–protein complex, the maximum number of intermolecular hydrogen bonds was also 4, observed at frames 265, 282, 300, 378, 459, 470, and 538, with an average of 1.854 hydrogen bonds. Similarly, the complex involving CID 11,500,585 reached a maximum of 4 hydrogen bonds at frames 47, 69, 535, and 917, with an average of 1.48 hydrogen bonds throughout the simulation. These findings indicate that CID 8768 exhibits the maximum number of hydrogen bonds among the compounds (Supplementary 6).

Ligand-Protein contacts analysis

During the SID, a comprehensive analysis was conducted on the affinity of the leads (CIDs 359, 8768, and 11500585), focusing on ligand atom interactions with protein residues complexed with the apoprotein. CID

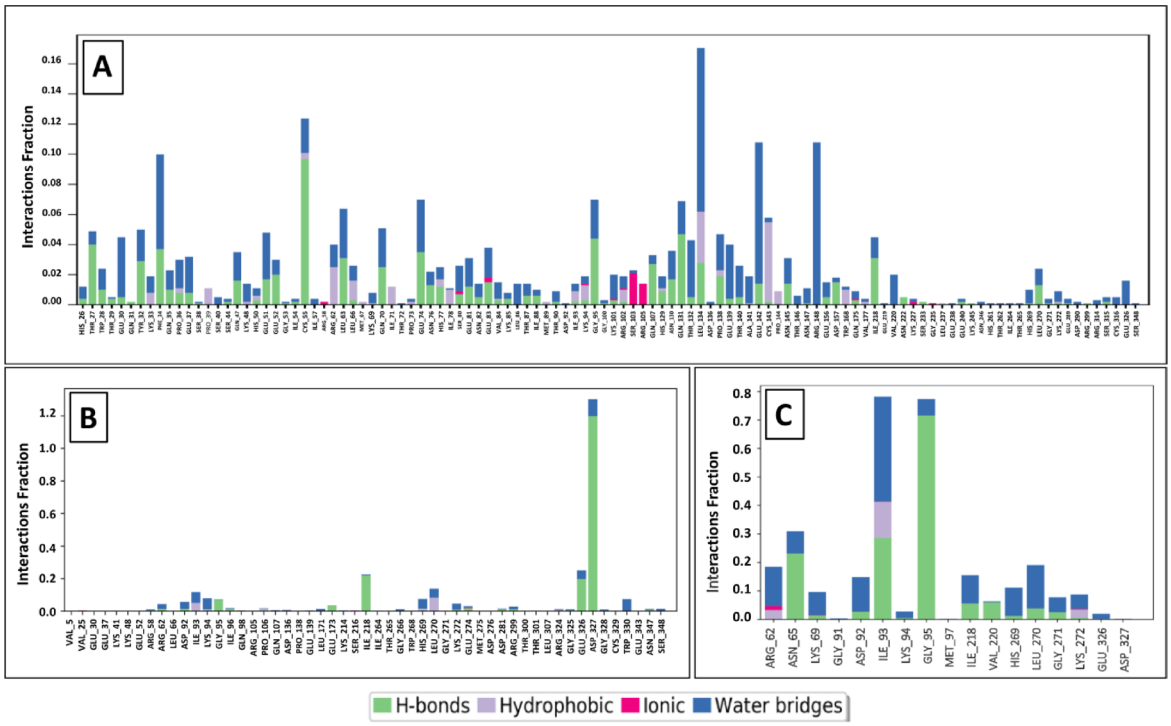

Fig. 8. The bar charts present the protein-ligand interactions from the 200 ns simulation, highlighting the binding of CID 359 (**A**), CID 8768 (**B**), and CID 11500585 (**C**) to the apoprotein.

8768 formed an H-bond with ASP_327 (Fig. 10B), and CID 11,500,585 formed an H-bond with GLY_95 (Fig. 10C). The compounds CID 8768 and 11,500,585 demonstrate better stability in ligand-protein interaction studies when compared to CID 359 (Fig. 10).

Post-simulation MM-GBSA

This study employed MM-GBSA techniques to evaluate the binding free energy of the protein-ligand complex over a 200-ns MD simulation trajectory. The binding free energy (ΔG Bind) of the lead compounds CID 359, CID 8768, and CID 11,500,585 was analyzed at both the initial (0 ns) and final (200 ns) stages of the simulation. The observed values ranged from − 22.41 kcal/mol to -13.66 kcal/mol for CID 359, -8.97 kcal/mol to -22.57 kcal/mol for CID 8768, and − 32.33 kcal/mol to -25.18 kcal/mol for CID 11,500,585, reflecting variations in binding stability over time (Fig. 11). Among them, CID 11,500,585 demonstrated the most favorable binding characteristics, consistently maintaining stable and strong interactions with the target protein throughout the simulation. This sustained binding stability highlights its potential as a promising candidate for further in-depth investigation (Supplementary 7).

Discussion

DENV remains a pressing global health concern, particularly due to the absence of targeted antiviral therapies, highlighting the need for new antiviral agents. The limitations of currently approved vaccines, such as CYD-TDV and TAK-003, which are restricted to specific populations[33,70]. Its complex nature, marked by diagnostic difficulties, persistence, prevalence, and atypical reservoirs, necessitates the exploration of alternative treatment approaches. This study targeted the NS1 protein (PDB ID: 4O6B) using an in-silico approach to find more effective antiviral drugs.

From the SWMD, 1,191 natural compounds were screened using molecular docking, narrowing down to 77 candidates. The top six, CIDs 359 (BE001), 8768 (RP004), 180,306 (GA011), 237,332 (RL333), 5,352,074 (RL462), and 11,500,585 (RR010), showed the highest docking scores (−5.567 to −4.55 kcal/mol) and were further analyzed through ADMET screening.

ADME properties influence drug mobility in the body, with drug discovery evaluating safety, efficacy, and bioavailability. High molecular mass drugs achieve good bioavailability with fewer rotatable bonds[71,72]. Lipinski's Rule-of-Five (RO5) suggests that a drug with molecular weight < 500 g/mol, logP < 5, and < 10 hydrogen-bond acceptors is likely to be orally active[73,74]. In ADME analysis, CID 180,306 violated Lipinski's rule due to its high molecular weight (804.11 g/mol), logP (6.65), and 6 hydrogen-bond donors, while the other five compounds (CIDs 359, 8768, 237332, 5352074, and 11500585) passed the ADME evaluation.

Toxicity analysis shows that CIDs 11,500,585, 359, and 8768 exhibited minimal toxicity across most organ systems, indicating excellent safety potential. However, CID 359 showed cardiotoxicity, requiring modification for improved safety. CID 180,306 displayed multiple toxicities, making it less viable. Based on safety profiles, CIDs 359, 8768, and 11,500,585 are proposed as lead compounds for further evaluation.

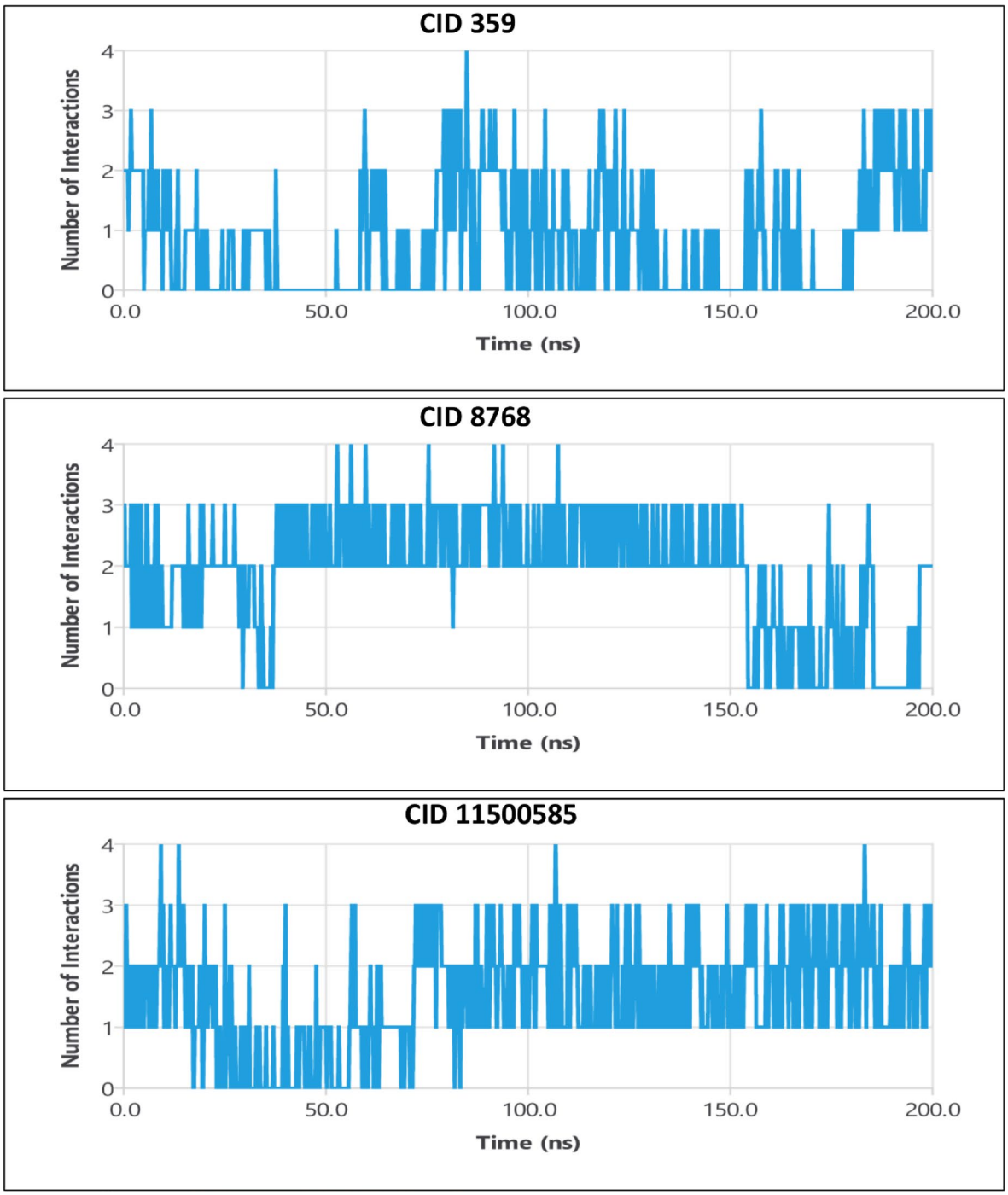

Fig. 9. Analysis of intermolecular hydrogen bonds between the ligand and the protein.

Molecular docking analysis reveals strong interactions among CIDs 359, 8768, and 11,500,585 with the target protein. Among all three compounds, common residues, ILE93 and ILE218, were identified as key contributors to hydrophobic interactions, suggesting binding to the same active site of the protein. Additionally, two compounds (CIDs 359, 8768) commonly formed hydrogen bonds with ILE93 and ILE218, further emphasizing their binding potential. A BLAST analysis followed by multiple sequence alignment with homologous proteins confirmed that the interacting residues are located within conserved regions.

MM-GBSA analysis revealed strong binding affinities between the lead compounds and NS1. The lower ΔG Bind values indicate a stronger binding affinity[75]. CID 11,500,585 exhibits the most favorable interaction (−27.7 kcal/mol), which confirms its potential as a promising candidate for further investigation. In addition to confirming the docking results, this energy profile points to extended binding that would impair NS1's ability to replicate viruses and evade the immune system.

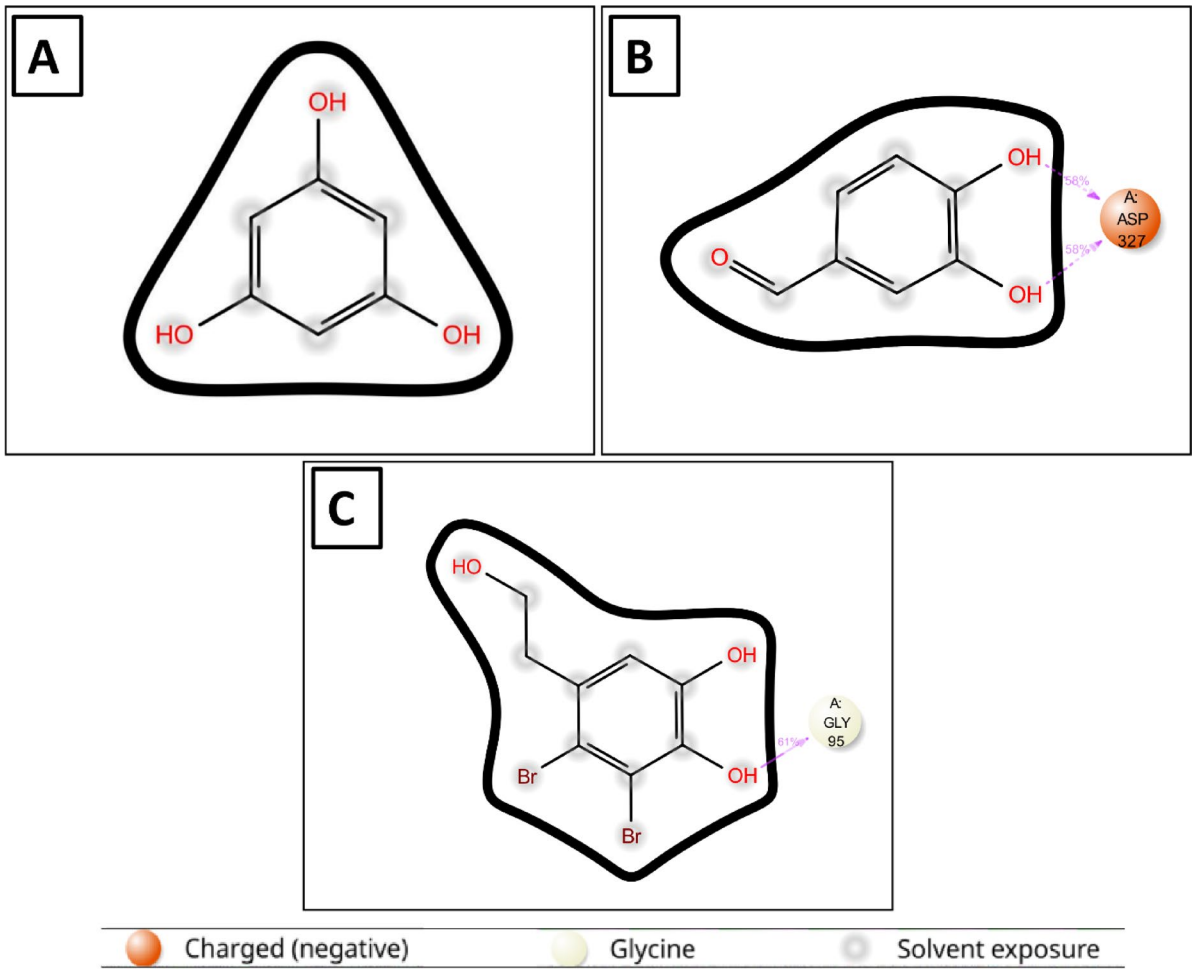

Fig. 10. Illustration showing the results of interactions between proteins and ligands obtained after molecular dynamics simulation. Documented are the following CIDs: 359 (**A**), 8768 (**B**), and 11500585 (**C**).

DFT, a quantum mechanical approach, provides insights into the electronic structure of molecules[76]. Hard molecules generally exhibit a larger HOMO-LUMO energy gap, signifying lower chemical reactivity, whereas softer molecules possess a smaller energy gap contributing to enhanced stability[60,77,78]. A molecule's reactivity is indicated by a reduced energy gap, which increases the binding affinity to the active site of the NS1 protein. A greater gap indicates chemical stability, but it also implies a lower reactivity, which could potentially diminish antiviral activity. The inhibitory potential of hard molecules is higher due to their reduced hardness. Softer molecules are more reactive, which may result in improved binding conformations and an increase in antiviral activity[79,80].

Based on the HOMO-LUMO energy gap, the lead compound CID 8768 (4.43 eV) exhibits the highest chemical reactivity, which may enhance its potential antiviral interactions. In contrast, CIDs 359 (6.24 eV) and 11,500,585 (5.16 eV) demonstrate greater chemical stability due to their wider energy gaps. Notably, their higher hardness values (3.12 and 2.58, respectively) suggest lower reactivity and limited electron exchange capacity, which may reduce their inhibitory efficiency if the antiviral mechanism relies on strong electronic interactions with the NS1 protein. However, their stability and structural rigidity could still support selective binding, indicating their potential as stable yet possibly less reactive antiviral candidates.

The leads show several common biological activities that could be key to stopping the dengue virus from spreading. For example, as MIA, they might disrupt the virus' ability to enter cells by altering the cell membranes[81]. The JAK2 expression inhibitors could help reduce the inflammatory processes that often boost viral replication[82]. According to QSAR, CID 11,500,585 exhibits antiviral activities similar to those effective against viruses like Adenovirus, CMV, and Herpes, which suggests they could target and show broad-spectrum activity against DNA and RNA viruses, influencing host immunity and viral replication. Together, these biological effects point to the lead's potential to block the virus at multiple stages, preventing its entry into cells, stopping its replication, and halting its spread.

MD simulation analysis revealed key stability parameters for the leads. CID 359, exhibited an average protein RMSD of 4.368 Å, ligand RMSD of 0.0885 Å, RMSF of 1.468 Å, Rg of 2.112 Å, SASA of 154.021 $Å^2$, and formed 266 hydrogen bonds with the protein. CID 8768, showed an average protein RMSD of 7.135 Å, ligand RMSD of 0.3787 Å, RMSF of 6.763 Å, Rg of 2.323 Å, SASA of 146.410 $Å^2$, and 268 hydrogen bonds. The unusually

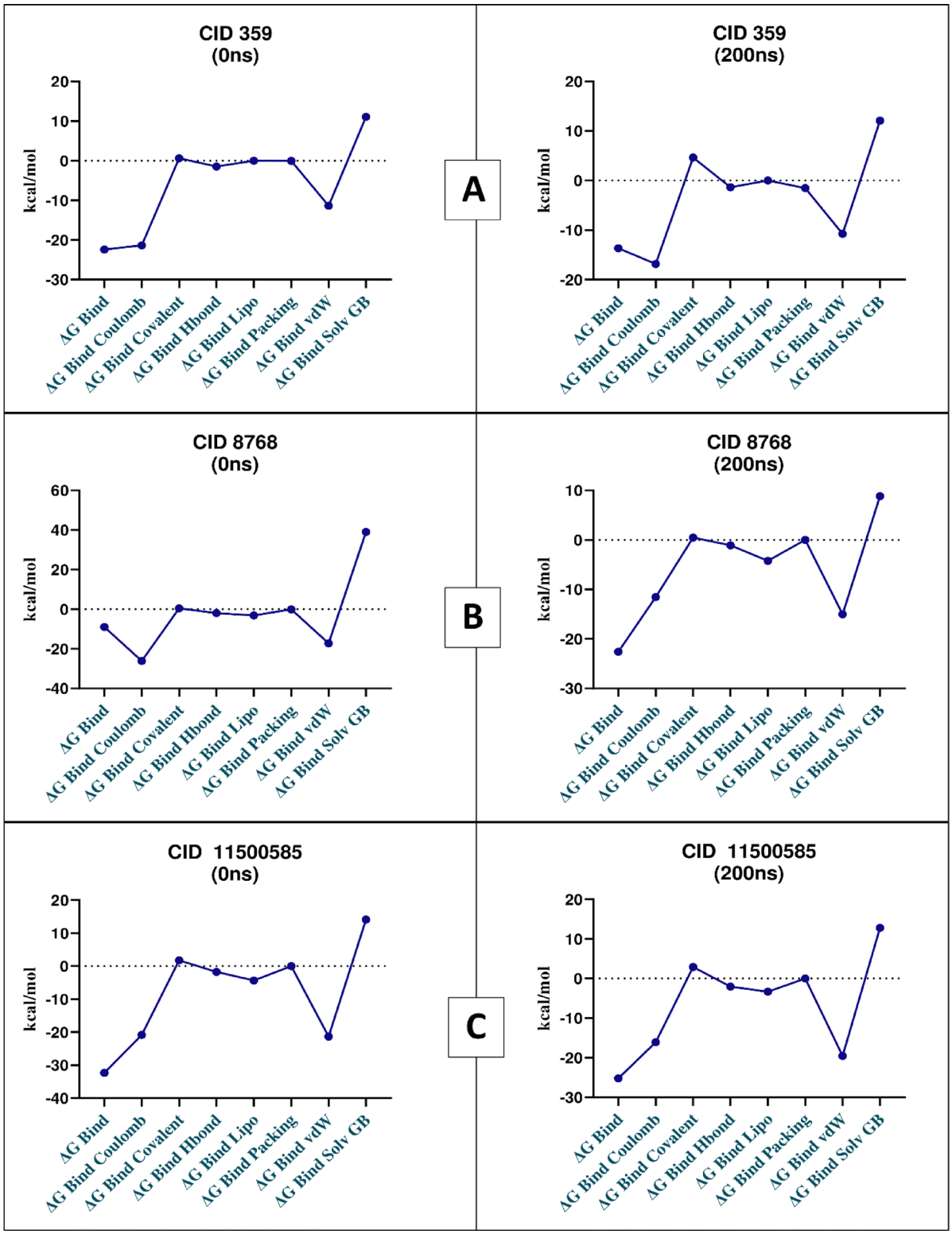

Fig. 11. The graphs depict the changes in binding free energy for the lead compounds CID 359 (**A**), CID 8768 (**B**), and CID 11500585 (**C**) at both the initial (0 ns) and final (200 ns) stages of the 200 ns MD simulation.

high RMSD and RMSF values observed for CID 8768 may indicate a poor binding orientation, partial ligand dissociation, or instability within the binding pocket. CID 11,500,585, demonstrated an average protein RMSD of 3.838 Å, ligand RMSD of 0.6934 Å, RMSF of 1.247 Å, Rg of 2.709 Å, SASA of 106.230 $Å^2$, and 265 hydrogen bonds with the protein. All of these values indicate a stable conformation and deep binding within the NS1 active site. The robustness of this interaction is critical, as sustained inhibition of NS1 could neutralize its intracellular

cofactor role and extracellular immune-modulatory effects, as supported by studies indicating NS1's role in vascular leakage and cytokine overproduction. Analysis of protein-ligand and ligand-protein interactions confirmed that all three leads establish hydrogen bonds, hydrophobic interactions, and water bridges reinforcing their stable association with the target protein.

Post-simulation MM-GBSA analysis revealed the binding free energies of the leads. At the initial stage, the binding energies were −22.41, −8.97, and −32.33 kcal/mol, respectively, whereas at the final stage, they were −13.66, −22.57, and −25.18 kcal/mol. These variations indicate changes in binding stability throughout the simulation, providing insights into the dynamic behaviour of the protein-ligand complexes. CID 11,500,585 maintained constant binding, a crucial requirement for candidate optimisation in structure-based drug design, in contrast to CID 359 and CID 8768, which displayed noticeable fluctuations.

Based on the comprehensive analysis of docking, ADMET screening, post-docking MM-GBSA, HOMO-LUMO gap evaluation, PASS prediction, and overall MD simulation results, CID 11,500,585 exhibited the highest stability. Its consistent binding affinity and favorable pharmacokinetic properties suggest its potential as a promising drug candidate. This compound demonstrated negative binding free energy values of −27.7 kcal/mol in post-docking MM-GBSA analysis and −25.18 kcal/mol in post-simulation MM-GBSA analysis. Notably, CID 11,500,585 consistently exhibited the most negative binding free energy across both analyses. The robust and sustained interaction with the NS1 protein underscores its potential as a promising candidate for therapeutic development.

Because of the absence of FDA-approved drugs targeting the NS1 protein of DENV, the identification of novel inhibitors is necessary. Three leads CIDs 359 (Phloroglucinol), 8768 (Protocatechualdehyde), and 11,500,585 (3,4-dibromo-5-(2-hydroxyethyl) benzene-1,2-diol) were analyzed, each possessing distinct structural and functional properties. Among them, 3,4-dibromo-5-(2-hydroxyethyl)benzene-1,2-diol (RR059) (Fig. 12), a phytochemical derived from the marine red alga *Rhodomela confervoides*, belonging to the Rhodomelaceae

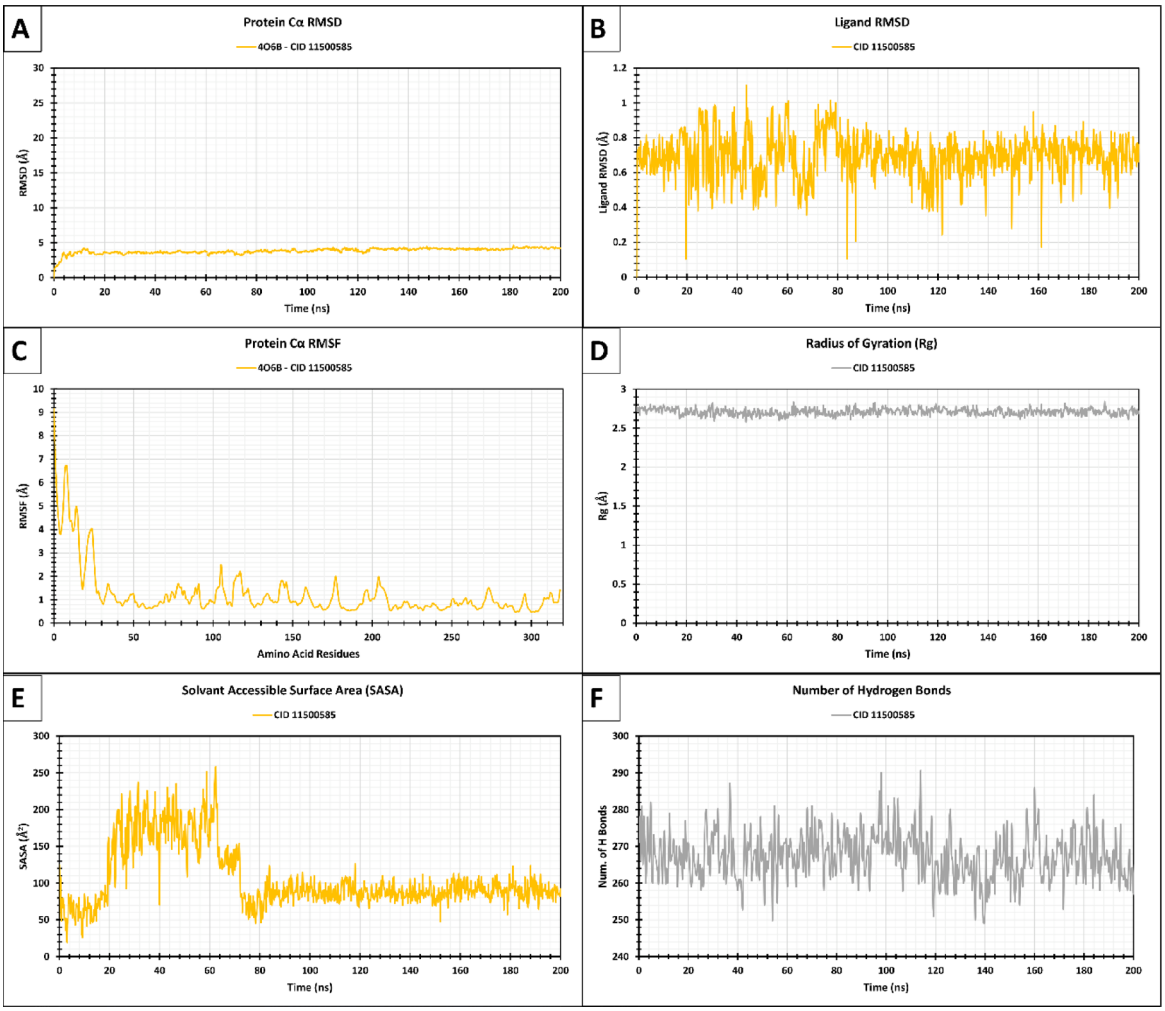

Fig. 12. All MD simulation parameters of the final lead compound (CID 11500585) in complex with the target protein (PDB ID: 4O6B) over a 200 ns trajectory. Shown are: (**A**) protein Cα RMSD, (**B**) ligand RMSD, (**C**) protein Cα RMSF, (**D**) radius of gyration (Rg), (**E**) solvent accessible surface area (SASA), and (**F**) number of hydrogen bonds.

family, exhibits significant antioxidant activity, which may contribute to viral inhibition, suggesting potential therapeutic applications[83–86].

Previous studies have explored the antiviral properties of Dragon fruit seed phytochemicals and the antiviral potential of Jaceidin, Centaureidin, Artecanin, Secotanaparthenolide, Artematin, Schizolaenone B, Isopomiferin, 6,8-Diprenyleriodictyol, and Anthraxin against DENV[87,88]. Additionally, a study analyzed the antiviral effects of four seaweed extracts (Phaeophyta: *Padina gymnospora*, *Canistrocarpus cervicornis*; Chlorophyta: *Caulerpa racemosa;* Rhodophyta: *Palisada perforate*) against the dengue virus using in-silico approaches[89]. However, there has been no previous investigation that has conducted a thorough computational analysis of marine-derived metabolites aimed at the conserved regions of the NS1 protein in DENV, making this study a novel contribution to the field. The compounds identified in this study, which target the pathogen, have not been reported in any previous research. These compounds are entirely novel and distinct from those discussed in existing studies.

This study is the first to specifically mention using combined computer tools, like molecular docking, MM-GBSA, ADMET, DFT, PASS prediction, and MD simulation, on the NS1 protein in *Rhodomela confervoides*. The findings presented here introduce unexplored compounds as potential NS1 inhibitors, offering a novel contribution to antiviral drug discovery.

This research was conducted as a self-initiated project without external financial support. Due to limited laboratory facilities and funding constraints, experimental validation could not be performed, and no in vitro or in vivo activity was carried out. Control cannot be implemented due to the absence of FDA-approved medications. Consequently, data validation with established inhibitors is absent; yet, this investigation may further the identification of a novel therapeutic drug. Nevertheless, these findings provide a reliable framework for future wet-lab validation. The integration of these in silico insights with upcoming in vitro and in vivo assays will significantly advance the development of targeted antiviral therapies against dengue.

Conclusion

This study utilized an in-silico method to identify a more effective antiviral drug for DENV, screening 1,191 seaweed metabolite compounds and finding promising therapeutic agents derived from seaweeds due to a lack of FDA-approved medication. The study identifies three compounds for further investigation: CIDs 359, 8768, and 11,500,585. The compound CID 11,500,585 (3,4-dibromo-5-(2-hydroxyethyl) benzene-1,2-diol) from *Rhodomela confervoides* seaweed, which is indigenous to Dalian, Liaoning Province, Republic of China, was chosen because it has a better ADME profile, is less toxic, and has a higher molecular docking affinity. It has also shown promising results in MM-GBSA, HOMO-LUMO analysis, QSAR, and enhanced MD simulation outcomes. Before the compound can be approved for therapeutic use, it needs to be tested further in vivo and in vitro to make sure it works against the target protein.

Materials and methods

Preparation of target protein and ligand

The protein structure of dengue viruses having PDB ID: 4O6B was downloaded from the RCSB Protein Data Bank (https://www.rcsb.org/) in PDB format[90]. The X-ray diffraction method yielded the acquired protein's atomic and molecular structure, having a value-free score of 0.217 and a resolution value of 3.00 Å. The B chain, co-crystallized ligand, and heteroatoms were deleted from the obtained protein structure, which comprised A and B chains with a total amino acid sequence length of 376, for further preparation using Schrödinger 2023-1's protein preparation wizard[91]. Thus, A chain was created by assigning missing side chains and using the OPLS4 Force Field, allocating hydrogen bonds, setting the binding order, as well as the elimination of water molecules found in the default parameter of the Protein Preparation Wizard (Fig. 13)[91,92]. Consequently, a total of 1191 seaweed metabolite compounds extracted from the seaweed metabolite database (https://www.swmd.co.in/) were processed by the LigPrep function of Maestro 13.5 [92]. Protein protonation states were assigned using PROPKA at pH 7.4, while ligand protonation was performed using Epik 5.3 at pH 7.0 [93].

Computational assessment of protein-ligand binding affinity through molecular Docking

Molecular docking is a computational method used to analyze binding affinities and molecular interactions between a target protein and a drug candidate[61,94,95]. It quantifies binding affinity by assessing ligand-receptor interactions in a protein-ligand complex[96]. Due to the absence of a co-crystallized ligand for the target protein, blind docking was carried out as an alternative to site-specific docking. Site-specific docking could have been conducted if a co-crystallized ligand had been present. A grid box for docking was generated using the receptor grid feature in the Schrödinger Suite[97]. Blind docking was performed to cover the entire protein, and the grid box dimensions were set at X= −11.117 Å, Y= −31.193 Å, and Z= -8.593 Å. The grid box size was (x range × y range × z range) = 30 Å × 30 Å × 30 Å. This technique involved docking 1191 seaweed compounds with the prepared target protein using Glide 2023 and Maestro 13.5 of Schrödinger Desmond software[98,99]. Throughout the docking procedure, OPLS4 was utilised as a force field in standard precision mode[100]. The Maestro viewer displayed diverse types of chemical bonds and residues that interact with ligands[94].

BLASTp and multiple sequence alignment were utilized to determine that the interacting ligands were binding to the conserved amino acid residues. To identify conserved amino acids in the NS1 protein, a BLASTp search was performed using the reference sequence. Multiple sequence alignment (MSA) of various DENV sequences was then done using Molecular Evolutionary Genetics Analysis (MEGA) v11 software (https://www.megasoftware.net/). Regions with high similarity were considered conserved. Finally, ligand-binding residues from docking were compared with these conserved residues.

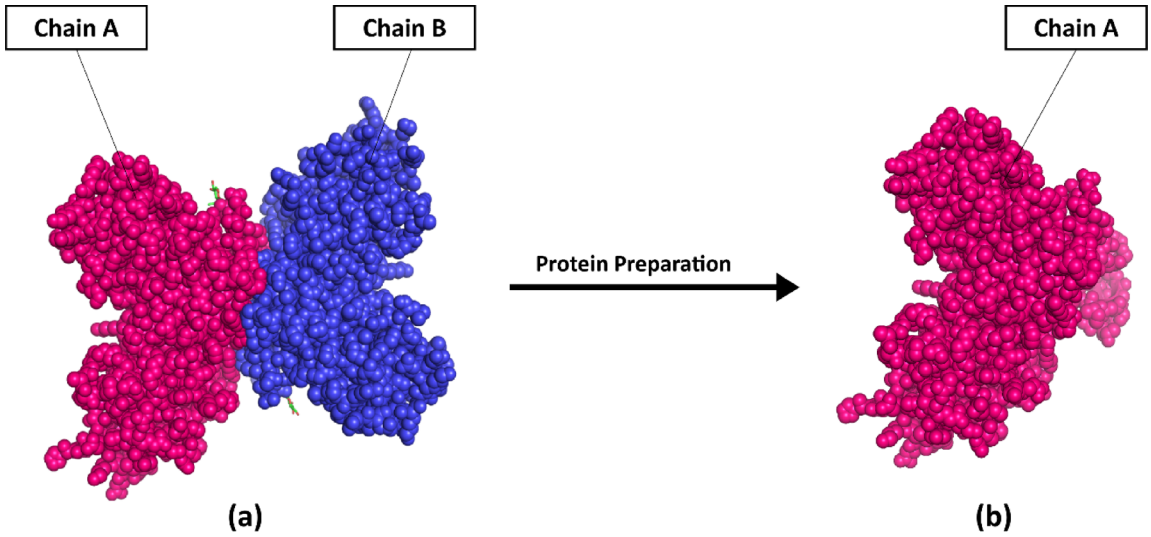

Fig. 13. The X-ray crystallographic structure of the Dengue Type 2 Virus (PDB ID: 4O6B) shows the side chains, heteroatoms, and the co-crystallized ligand (**a**); and the processed protein after removing the B chain, heteroatoms, and co-crystallized ligand (**b**).

Prediction of pharmacokinetics (PK) and toxicological profiles

In the in-silico approach, pharmacokinetics (PK) or ADME profile encompasses four key parameters: absorption, distribution, metabolism, and excretion, and these factors are crucial in assessing the potential success of a compound to be a drug[101]. All such factors were thoroughly examined by using the Swiss-ADME (www.swissadme.ch) online server, which provided predictions for gastrointestinal absorption, lipophilicity, solubility, and other drug-likeness characteristics of the selected compounds[74,102].

Toxicity assessment is another crucial step in computational drug design, where in-silico models predict chemical toxicity[67]. ProTox 3.0 (https://tox.charite.de/protox3/), a freely accessible internet server, was used to assess toxicity qualities and also aids in the assessment and forecasting of the compound's toxicity, related to hepatotoxicity, immunotoxicity, cytotoxicity, and other characteristics[67,103]. After analyzing the ADMET profiles of the top six compounds with the highest docking scores, lead compounds were identified from the top six compounds exhibiting excellent ADMET properties for further exploration.

Protein-ligand interaction analysis and calculation of Post-docking MM-GBSA

The selected lead compounds were analyzed through their docking complexes, with protein-ligand interactions visualized using Schrödinger Desmond's Maestro viewer, highlighting specific amino acids involved in binding.

After that, MM-GBSA analysis was conducted for post-docking binding energy calculations to refine interaction predictions[62,104,105]. Using the Prime MM-GBSA 3.0 module in Schrödinger's Maestro 13.5, analyzed binding free energy, binding interactions, and residues[94]. The selected lead compound's docked pose was assessed, where more negative binding free energy values indicated stronger stability[106,107]. This approach enhances drug candidate evaluation by providing a dynamic perspective beyond static docking.

Quantum mechanical (QM) calculation

Density Functional Theory (DFT) analysis was performed to investigate phytochemical reactivity and ligand-protein interactions using quantum mechanical principles[108]. QM calculations helped identify active conformations, binding affinity, and strain effects within the binding site. The study analyzed frontier molecular orbitals using Gaussian 6.0, focusing on HOMOs (electron donors) and LUMOs (electron acceptors)[109]. The HOMO-LUMO energy gap (ΔE), computed at the B3LYP/6-31G (d, p) level, indicated chemical stability and reactivity, where a larger ΔE signified high stability, and low reactivity[110]. The compounds exhibited greater hardness (η) than softness (S), which indicated better stability, while lower hardness and a more negative chemical potential suggested higher polarizability[111].

The electrophilicity index, crucial for identifying reactive sites, was determined based on HOMO-LUMO interactions and corresponding energy changes[112]. Key parameters were calculated as follows:

HOMO-LUMO Gap (ΔE) = ($E_{LUMO} - E_{HOMO}$).

Hardness (η) = (I – A)/2.

Softness (S) = 1/η.

Here, I (ionization potential) = $-E_{HOMO}$ and A (electron affinity) = $-E_{LUMO}$. A lower η indicates higher chemical reactivity[67,113]. These insights provide a deeper understanding of molecular stability and reactivity in ligand-protein interactions.

QSAR analysis

PASS (Prediction of Activity Spectra for Substances) is a computational tool designed to predict a range of biological activities, including pharmacological effects, toxicity risks, and mutagenicity, by analyzing structure-activity relationships to assess potential drug properties[114,115]. In this study, the biological spectrum of drug candidates was predicted using the Way2Drug platform (https://www.way2drug.com/passonline/predict.php), where the probability for active (Pa) and inactive (Pi) compounds ranges from 0.000 to 1.000. Pa > 0.7 suggests high activity and similarity to known pharmacological agents, values between 0.5 and 0.7 indicate moderate activity, whereas values below 0.5 recommend low or no activity[116,117].

Molecular dynamics simulation

MD simulations were performed to investigate the stability and behaviour of protein-ligand complexes within intricate biological environments[118]. Initially, molecular docking was performed to construct the protein-ligand complexes, followed by pre-processing using the Protein Preparation Wizard[119]. The binding capacity of selected compounds (CIDs 359, 8768, and 11500585) to the target protein was then analyzed through MD simulations to assess ligand stability. A 200ns MD simulation was executed utilizing Desmond (Schrödinger Suite) with the SPC water model within a $10 \times 10 \times 10$ Å^2 periodic bounding box. A 0.15 M salt concentration was maintained by randomly dispersing Na^+ and Cl^- ions throughout the solvated system[61,67]. The OPLS4 force field was applied to optimize the system, which was simulated under NPT conditions at 1.01325 bar pressure and 300.0 K temperature[67,94,100]. After system relaxation, the final output was recorded at 200 picoseconds(ps) intervals with an applied energy of 1.2 J[61]. Each system went through a typical two-phase equilibration procedure in Desmond prior to the production run. In order to permit solvent relaxation, an NVT equilibration was first carried out for 100 ps while placing positional constraints on the heavy solute atoms. The system was then able to modify its volume and achieve thermodynamic equilibrium at 300 K and 1 atm utilising the Nose–Hoover thermostat and Martyna–Tobias–Klein barostat after a 1 ns NPT equilibration without constraints.

Data availability

Data is contained within the article and Supplementary Material.

Received: 14 March 2025; Accepted: 5 August 2025
Published online: 01 October 2025

References

1. Chen, H. R. et al. Dengue virus nonstructural protein 1 induces vascular leakage through macrophage migration inhibitory factor and autophagy. *PLoS Negl. Trop. Dis.* **10**, 4828 (2016).
2. Alagarasu, K. et al. In vitro antiviral activity of potential medicinal plant extracts against dengue and Chikungunya viruses. *Front. Cell. Infect. Microbiol.* **12**, 866452 (2022).
3. Norshidah, H. et al. Assessing the potential of NS2B/NS3 protease inhibitors biomarker in curbing dengue virus infections: In silico vs In vitro approach. *Front. Cell. Infect. Microbiol.* **13**, 1–17 (2023).
4. Tan, B. E. K., Beard, M. R. & Eyre, N. S. Identification of key residues in dengue virus NS1 protein that are essential for its secretion. *Viruses* **15**, 1102 (2023).
5. Lee, P. X. et al. Relative contribution of nonstructural protein 1 in dengue pathogenesis. *J. Exp. Med.* **217**, 20191548 (2020).
6. Kok, B. H. et al. Dengue virus infection – a review of pathogenesis, vaccines, diagnosis and therapy. *Virus Res.* **324**, 199018 (2023).
7. Dwivedi, V. D., Tripathi, I. P. & Mishra, S. K. In silico evaluation of inhibitory potential of triterpenoids from azadirachta indica against therapeutic target of dengue virus, NS2B-NS3 protease. *J. Vector Borne Dis.* **53**, 156–161 (2016).
8. Bhatt, S. et al. The global distribution and burden of dengue. *Nature* **496**, 504–507 (2013).
9. Ding, J. et al. In-host modeling of dengue virus and non-structural protein 1 and the effects of ivermectin in patients with acute dengue fever. *CPT Pharmacometrics Syst. Pharmacol.* https://doi.org/10.1002/psp4.13233 (2024).
10. Rastogi, M., Sharma, N. & Singh, S. K. Flavivirus NS1: a multifaceted enigmatic viral protein. *Virol. J.* **13**, 131 (2016).
11. Avirutnan, P. *et al.* Secreted NS1 of Dengue Virus Attaches to the Surface of Cells via Interactions with Heparan Sulfate and Chondroitin Sulfate E. https://doi.org/10.1371/journal.ppat.0030183.
12. Kyle, J. L. & Harris, E. Global spread and persistence of dengue. *Annu. Rev. Microbiol.* **62**, 71–92 (2008).
13. Lee, K. S. et al. Dengue virus surveillance in Singapore reveals high viral diversity through multiple introductions and in situ evolution. *Infect. Genet. Evol.* **12**, 77–85 (2012).
14. Xia, H. et al. A cocrystal structure of dengue capsid protein in complex of inhibitor. *Proc. Natl. Acad. Sci. U. S. A.* **117**, 17992–18001 (2020).
15. Dayarathna, S. et al. Dengue NS1 interaction with lipids alters its pathogenic effects on monocyte derived macrophages. *J. Biomed. Sci.* **31**, 86 (2024).
16. Leitmeyer, K. C. et al. Dengue virus structural differences that correlate with pathogenesis. *J. Virol.* **73**, 4738–4747 (1999).
17. Reyes-Sandoval, A. & Ludert, J. E. The dual role of the antibody response against the flavivirus non-structural protein 1 (NS1) in protection and immuno-pathogenesis. *Front. Immunol.* **10**, 1651 (2019).
18. Glasner, D. R., Puerta-Guardo, H., Beatty, P. R. & Harris, E. The Good, the Bad, and the Shocking: The Multiple Roles of Dengue Virus Nonstructural Protein 1 in Protection and Pathogenesis. *Annu. Rev. Virol.* **5**, 227 (2018).
19. Somnuke, P., Hauhart, R. E., Atkinson, J. P., Diamond, M. S. & Avirutnan, P. N-linked glycosylation of dengue virus NS1 protein modulates secretion, cell-surface expression, hexamer stability, and interactions with human complement. *Virology* **413**, 253–264 (2011).
20. Sootichote, R. et al. Potential protective effect of dengue NS1 human monoclonal antibodies against dengue and Zika virus infections. *Biomedicines* https://doi.org/10.3390/biomedicines11010227 (2023).
21. Gonçalves, A. J. S. et al. Cooperation between CD4+ T cells and humoral immunity is critical for protection against dengue using a DNA vaccine based on the NS1 antigen. *PLoS Negl. Trop. Dis.* **9**, 4277 (2015).
22. Songprakhon, P. et al. Peptides targeting dengue viral nonstructural protein 1 inhibit dengue virus production. *Sci. Rep.* **10**, 12933 (2020).
23. Mackenzie, J. M., Jones, M. K. & Young, P. R. Immunolocalization of the dengue virus nonstructural glycoprotein NS1 suggests a role in viral RNA replication. *Virology* **220**, 232–240 (1996).
24. Avirutnan, P. et al. Antagonism of the complement component C4 by flavivirus nonstructural protein NS1. *J. Exp. Med.* **207**, 793–806 (2010).

25. Nasar, S., Iftikhar, S., Saleem, R., Nadeem, M. S. & Ali, M. The N and C-terminal deleted variant of the dengue virus NS1 protein is a potential candidate for dengue vaccine development. *Sci. Rep.* **14**, 1–11 (2024).
26. Modhiran, N. et al. Dengue virus NS1 protein activates cells via Toll-like receptor 4 and disrupts endothelial cell monolayer integrity. *Sci. Transl. Med.* **7**, 142 (2015).
27. Chao, C. H. et al. Dengue virus nonstructural protein 1 activates platelets via Toll-like receptor 4, leading to thrombocytopenia and hemorrhage. *PLOS Pathog.* **15**, e1007625 (2019).
28. Fatima, K. & Syed, N. I. Dengvaxia controversy: Impact on vaccine hesitancy. *J. Glob. Health* **8**, 20312 (2018).
29. Songprakhon, P. et al. Peptides targeting dengue viral nonstructural protein 1 inhibit dengue virus production. *Sci. Rep.* **10**, 12933 (2020).
30. Muller, D. A. & Young, P. R. The flavivirus NS1 protein: molecular and structural biology, immunology, role in pathogenesis and application as a diagnostic biomarker. *Antiviral Res.* **98**, 192–208 (2013).
31. Beatty, P. R. et al. Dengue virus NS1 triggers endothelial permeability and vascular leak that is prevented by NS1 vaccination. *Sci. Transl. Med.* **7**, 141 (2015).
32. Rajapakse, S., Rodrigo, C. & Rajapakse, A. Treatment of dengue fever. *Infect. Drug Resist.* **5**, 103 (2012).
33. Dengue and severe dengue. https://www.who.int/news-room/fact-sheets/detail/dengue-and-severe-dengue.
34. National Instite of Diabetes en Digestive and Kidney Diseases. Acetaminophen. *LiverTox Clin. Res. Inf. Drug-Induced Liver Inj.* (2016).
35. Campana, V. et al. Liver involvement in dengue: A systematic review. *Rev. Med. Virol.* **34**, e2564 (2024).
36. Simasathien, S. & Watanaveeradej, V. Dengue vaccine. *J. Med. Assoc. Thai.* **88**(Suppl 3), S363–S377 (2005).
37. Sridhar, S. et al. Effect of dengue serostatus on dengue vaccine safety and efficacy. *N. Engl. J. Med.* **379**, 327–340 (2018).
38. Lee, M. F., Long, C. M. & Poh, C. L. Current status of the development of dengue vaccines. *Vaccine X* **22**, 100604 (2025).
39. Ahmed, I., Ahamed, R., Nahar, S. & Bari, L. F. Immunization against dengue virus infection is coercive: A timely call. *Health Sci. Reports* **7**, 2170. https://doi.org/10.1002/hsr2.2170 (2024).
40. Vaccines and immunization: Dengue. https://www.who.int/news-room/questions-and-answers/item/dengue-vaccines.
41. Dengue Tetravalent Vaccine (Live, Attenuated) Takeda - opinion on medicine for use outside EU | European Medicines Agency (EMA). https://www.ema.europa.eu/en/opinion-medicine-use-outside-EU/human/dengue-tetravalent-vaccine-live-attenuated-takeda.
42. Percio, J. et al. Safety signal detected: Anaphylaxis after attenuated dengue vaccine (TAK-003) - Brazil, march 1, 2023-march 11, 2024. *Vaccine* **42**, 126407 (2024).
43. Qdenga | European Medicines Agency (EMA). https://www.ema.europa.eu/en/medicines/human/EPAR/qdenga?utm.
44. Pierce, K. K. et al. TV005 dengue vaccine protects against dengue serotypes 2 and 3 in two controlled human infection studies. *J. Clin. Invest.* **134**, e173328 (2024).
45. Dengue Vaccines — Vax-Before-Travel. https://www.vax-before-travel.com/dengue-vaccines.
46. Walsh, M. C. R. et al. Safety and durable immunogenicity of the TV005 tetravalent dengue vaccine, across serotypes and age groups, in dengue-endemic Bangladesh: a randomised, controlled trial. *Lancet. Infect. Dis.* **24**, 150–160 (2024).
47. Laille, M., Gerald, F. & Debitus, C. In vitro antiviral activity on dengue virus of marine natural products. *Cell. Mol. Life Sci.* **54**, 167–170 (1998).
48. Wu, D. L. et al. Polyketides and alkaloids from the marine-derived fungus Dichotomomyces cejpii F31–1 and the antiviral activity of scequinadoline A against dengue virus. *Mar. Drugs* **16**, 229 (2018).
49. Hans, N., Malik, A. & Naik, S. Antiviral activity of sulfated polysaccharides from marine algae and its application in combating COVID-19: Mini review. *Bioresour Technol. Reports* **13**, 100623 (2021).
50. Lomartire, S. & Gonçalves, A. M. M. Antiviral activity and mechanisms of seaweeds bioactive compounds on enveloped viruses—a review. *Mar. Drugs* **20**, 385 (2022).
51. dos Santos, G. S. et al. Seaweeds and Corals from the Brazilian Coast: Review on biotechnological potential and environmental aspects. *Molecules* **28**, 4285 (2023).
52. Lomartire, S. et al. Environmental impact on seaweed phenolic production and activity: An important step for compound exploitation. *Mar. Drugs* **19**, 245 (2021).
53. Sharma, B., Bhattacherjee, D., Zyryanov, G. V. & Purohit, R. An insight from computational approach to explore novel, high-affinity phosphodiesterase 10A inhibitors for neurological disorders. *J. Biomol. Struct. Dyn.* **41**, 9424–9436 (2023).
54. Sharma, B. & Purohit, R. Enhanced sampling simulations to explore himalayan phytochemicals as potential phosphodiesterase-1 inhibitor for neurological disorders. *Biochem. Biophys. Res. Commun.* **758**, 151614 (2025).
55. Kalsi, N., Gopalakrishnan, C., Rajendran, V. & Purohit, R. Biophysical aspect of phosphatidylinositol 3-kinase and role of oncogenic mutants (E542K & E545K). *J. Biomol. Struct. Dyn.* **34**, 2711–2721 (2016).
56. Kumar, A., Rajendran, V., Sethumadhavan, R. & Purohit, R. Relationship between a point mutation S97C in CK1δ protein and its affect on ATP-binding affinity. *J. Biomol. Struct. Dyn.* **32**, 394–405 (2014).
57. Kamaraj, B., Rajendran, V., Sethumadhavan, R. & Purohit, R. In-silico screening of cancer associated mutation on PLK1 protein and its structural consequences. *J. Mol. Model.* **19**, 5587–5599 (2013).
58. Drug Toxicity - an overview | ScienceDirect Topics. https://www.sciencedirect.com/topics/pharmacology-toxicology-and-pharmaceutical-science/drug-toxicity.
59. Basu, S., Veeraraghavan, B. & Anbarasu, A. Anti-bacterial compounds from Indian curry-leaf tree Murraya koenigii have potential to inhibit carbapenem-resistant Streptococcus pneumoniae. *Clin. Epidemiol. Glob. Heal.* **28**, 101511 (2024).
60. Miar, M., Shiroudi, A., Pourshamsian, K., Oliaey, A. R. & Hatamjafari, F. Theoretical investigations on the HOMO–LUMO gap and global reactivity descriptor studies, natural bond orbital, and nucleus-independent chemical shifts analyses of 3-phenylbenzo[d] thiazole-2(3H)-imine and its para-substituted derivatives: Solvent and substituent effects. *J. Chem. Res.* **45**, 147–158 (2021).
61. Saha, O. et al. Antiviral activity, pharmacoinformatics, molecular docking, and dynamics studies of Azadirachta indica Against Nipah virus by targeting envelope glycoprotein: Emerging strategies for developing antiviral treatment. *Bioinform. Biol. Insights* **18**, 11779322241264144 (2024).
62. Siddiquee, N. H. et al. Unveiling the antiviral activity of 2′,3,5,7-Tetrahydroxyflavanone as potential inhibitor of chikungunya virus envelope glycoprotein. *Inform. Med. Unlocked* **47**, 101486 (2024).
63. Siddiquee, N. H. et al. Nature's defense against emerging neurodegenerative threats: Dynamic simulation, PCA, DCCM identified potential plant-based antiviral lead targeting borna disease virus nucleoprotein. *PLoS ONE* **19**, e0310802 (2024).
64. Siddiquee, N. H. et al. In-silico identification of novel natural drug leads against the Ebola virus VP40 protein: A promising approach for developing new antiviral therapeutics. *Inform. Med. Unlocked* **45**, 101458 (2024).
65. Hassan, A. M. et al. Evaluating the binding potential and stability of drug-like compounds with the Monkeypox Virus VP39 protein using molecular dynamics simulations and free energy analysis. *Pharmaceuticals* **17**, 1617 (2024).
66. Boulaamane, Y. et al. Computational screening of natural products as tryptophan 2,3-dioxygenase inhibitors: Insights from CNN-based QSAR, molecular docking, ADMET, and molecular dynamics simulations. *Comput. Biol. Med.* **191**, 110199 (2025).
67. Talukder, M. E. K. et al. Molecular docking, QSAR, and simulation analyses of EGFR-targeting phytochemicals in non-small cell lung cancer. *J. Mol. Struct.* **1321**, 139924 (2025).
68. Zia, S. et al. Potential inhibitors of lumpy skin disease's viral protein (DNA polymerase): A combination of bioinformatics approaches. *Animals* **14**, 1283 (2024).

69. Siddiquee, N. H. et al. Natural products in precision neurological disease (Cryptococcal Meningitis): Structure-based phytochemical screening of Glycyrrhiza glabra plant against cryptococcus neoformans farnesyltransferase (FTase). *Chem. Biodivers.* **1**, 17. https://doi.org/10.1002/cbdv.202401987 (2025).
70. Pourzangiabadi, M., Najafi, H., Fallah, A., Goudarzi, A. & Pouladi, I. Dengue virus: Etiology, epidemiology, pathobiology, and developments in diagnosis and control – A comprehensive review. *Infect. Genet. Evol.* **127**, 105710 (2025).
71. Evaluation of blockbuster drugs under the rule-of-five - PubMed. https://pubmed.ncbi.nlm.nih.gov/20225662/.
72. Sadgrove, N. J. & Jones, G. L. From petri dish to patient: Bioavailability estimation and mechanism of action for antimicrobial and immunomodulatory natural products. *Front. Microbiol.* **10**, 2470 (2019).
73. Lipinski, C. A. Lead- and drug-like compounds: The rule-of-five revolution. *Drug Discov. Today Technol.* **1**, 337–341 (2004).
74. Siddiquee, N. H. et al. Molecular activity of bioactive phytocompounds for inhibiting host cell attachment and membrane fusion interacting with West Nile Virus envelope glycoprotein. *PLoS ONE* **20**, e0321902 (2025).
75. Zhang, X., Perez-Sanchez, H. & Lightstone, C. F. A. Comprehensive docking and MM/GBSA rescoring study of ligand recognition upon binding antithrombin. *Curr. Top. Med. Chem.* **17**, 1631–1639 (2017).
76. Regina, O. A. Quantum mechanical methods in computational chemistry. *Idosr J. Comput. Appl. Sci.* **9**, 6–10 (2024).
77. Jáafaru, S. C. et al. In-silico exploration and structure-based design of Praziquantel derivatives as potential inhibitors of schistosoma mansoni Glutathione S-transferase (SmGST). *Sci. African* **24**, 2169 (2024).
78. Hadigheh Rezvan, V. Molecular structure, HOMO–LUMO, and NLO studies of some quinoxaline 1,4-dioxide derivatives: Computational (HF and DFT) analysis. *Results Chem.* **7**, 101437 (2024).
79. Chtita, S. et al. QSAR study of N -substituted oseltamivir derivatives as potent avian influenza virus H5N1 inhibitors using quantum chemical descriptors and statistical methods. *New J. Chem.* **44**, 1747–1760 (2020).
80. Alam, M. et al. Synthesis, characterization, antibacterial activity of thiosemicarbazones derivatives and their computational approaches: Quantum calculation, molecular docking, molecular dynamic, ADMET. *QSAR. Heliyon* **9**, e16222 (2023).
81. Harada, S. The broad anti-viral agent glycyrrhizin directly modulates the fluidity of plasma membrane and HIV-1 envelope. *Biochem. J.* **392**, 191–199 (2005).
82. Wang, J., Prinz, R. A., Liu, X. & Xu, X. In vitro and in vivo antiviral activity of gingerenone a on influenza a virus is mediated by targeting Janus Kinase 2. *Viruses* **12**, 1141 (2020).
83. Davis, G. D. J. & Vasanthi, A. H. R. Seaweed metabolite database (SWMD): A database of natural compounds from marine algae. *Bioinformation* **5**, 361–364 (2011).
84. Li, K., Li, X. M., Gloer, J. B. & Wang, B. G. Isolation, characterization, and antioxidant activity of bromophenols of the marine red alga Rhodomela confervoides. *J. Agric. Food Chem.* **59**, 9916–9921 (2011).
85. Peterhans, E. Oxidants and antioxidants in viral diseases: Disease mechanisms and metabolic regulation. *J. Nutr.* **127**, 962S-965S (1997).
86. WoRMS - World Register of Marine Species - Rhodomela confervoides (Hudson) P.C.Silva, 1952. https://www.marinespecies.org/aphia.php?p=taxdetails&id=144854.
87. Sathyamurthy, B. & Sushmitha, H. S. In Silico drug designing studies on dengue virus NS1 protein. *PharmaTutor* **6**, 31 (2018).
88. Qaddir, I., Majeed, A., Hussain, W., Mahmood, S. & Rasool, N. An *in silico* investigation of phytochemicals as potential inhibitors against non-structural protein 1 from dengue virus 4. *Brazilian J. Pharm. Sci.* **56**, e17420 (2020).
89. Koishi, A. C. et al. Screening of dengue virus antiviral activity of marine seaweeds by an in situ enzyme-linked immunosorbent assay. *PLoS ONE* **7**, 51089 (2012).
90. Akey, D. L. et al. Flavivirus NS1 structures reveal surfaces for associations with membranes and the immune system. *Science* **80**(343), 881–885 (2014).
91. MadhaviSastry, G., Adzhigirey, M. & Day, T. Annabhimoju, R. & Sherman, W. Protein and ligand preparation: Parameters, protocols, and influence on virtual screening enrichments. *J. Comput. Aided. Mol. Des.* **27**, 221–234 (2013).
92. Lu, C. et al. OPLS4: improving force field accuracy on challenging regimes of chemical space. *J. Chem. Theory Comput.* **17**, 4291–4300 (2021).
93. Shelley, J. C. et al. Epik: A software program for pKa prediction and protonation state generation for drug-like molecules. *J. Comput. Aided. Mol. Des.* **21**, 681–691 (2007).
94. Ahammad, F. et al. Pharmacoinformatics and molecular dynamics simulation-based phytochemical screening of neem plant (Azadiractha indica) against human cancer by targeting MCM7 protein. *Brief. Bioinform.* **22**, 1–15 (2021).
95. Saha, O. et al. Antiviral activity, pharmacoinformatics, molecular docking, and dynamics studies of Azadirachta indica against Nipah virus by targeting envelope glycoprotein: Emerging strategies for developing antiviral treatment. *Bioinform. Biol. Insights* **18**, 11779322241264144 (2024).
96. Debroy, R. & Ramaiah, S. MurC ligase of multi-drug resistant Salmonella Typhi can be inhibited by novel Curcumin derivative: Evidence from molecular docking and dynamics simulations. *Int. J. Biochem. Cell Biol.* **151**, 106279 (2022).
97. Meng, X.-Y., Zhang, H.-X., Mezei, M. & Cui, M. Molecular docking: A powerful approach for structure-based drug discovery. *Curr. Comput. Aided-Drug Des.* **7**, 146–157 (2012).
98. Ogbodo, U. C. et al. Computational identification of potential inhibitors targeting cdk1 in colorectal cancer. *Front. Chem.* **11**, 1–17 (2023).
99. Pires, D. E. V., Blundell, T. L. & Ascher, D. B. pkCSM: Predicting small-molecule pharmacokinetic and toxicity properties using graph-based signatures. *J. Med. Chem.* **58**, 4066–4072 (2015).
100. Friesner, R. A. et al. Glide: a new approach for rapid, accurate docking and scoring. 1. Method and assessment of docking accuracy. *J. Med. Chem.* **47**, 1739–1749 (2004).
101. Harder, E. et al. OPLS3: A force field providing broad coverage of drug-like small molecules and proteins. *J. Chem. Theory Comput.* **12**, 281–296 (2016).
102. Tung, B. T., Son, N. N., Kim, N. B., Khanh, D. T. H. & Minh, P. H. In silico screening of alkaloids as potential inhibitors of HER2 protein for breast cancer treatment. *Vietnam J. Chem.* **61**, 308–317 (2023).
103. Siddiquee, N. H. et al. Insights into novel inhibitors intending HCMV protease a computational molecular modelling investigation for antiviral drug repurposing. *Inform. Med. Unlocked* **48**, 101522 (2024).
104. Talukder, M. E. K. et al. Molecular docking, QSAR, and simulation analyses of EGFR-targeting phytochemicals in non-small cell lung cancer. *J. Mol. Struct.* **1321**, 139924 (2025).
105. Banerjee, P., Eckert, A. O., Schrey, A. K. & Preissner, R. ProTox-II: a webserver for the prediction of toxicity of chemicals. *Nucleic Acids Res.* **46**, W257–W263 (2018).
106. Godschalk, F., Genheden, S., Söderhjelm, P. & Ryde, U. Comparison of MM/GBSA calculations based on explicit and implicit solvent simulations. *Phys. Chem. Chem. Phys.* **15**, 7731–7739 (2013).
107. Sgobba, M., Caporuscio, F., Anighoro, A., Portioli, C. & Rastelli, G. Application of a post-docking procedure based on MM-PBSA and MM-GBSA on single and multiple protein conformations. *Eur. J. Med. Chem.* **58**, 431–440 (2012).
108. Chen, D. et al. Regulation of protein-ligand binding affinity by hydrogen bond pairing. *Sci. Adv.* **2**, e1501240 (2016).
109. Genheden, S. & Ryde, U. The MM/PBSA and MM/GBSA methods to estimate ligand-binding affinities. *Expert Opin. Drug Discov.* **10**, 449–461 (2015).
110. Majeed, A., Hussain, W., Yasmin, F., Akhtar, A. & Rasool, N. Virtual screening of phytochemicals by targeting HR1 domain of SARS-CoV-2 S protein: Molecular docking, molecular dynamics simulations, and DFT studies. *Biomed Res. Int.* **2021**, 6661191 (2021).

111. Samad, A., Huq, M. A. & Rahman, M. S. Bioinformatics approaches identified dasatinib and bortezomib inhibit the activity of MCM7 protein as a potential treatment against human cancer. *Sci. Rep.* **12**, 1–16 (2022).
112. Rijal, R., Lamichhane, H. P. & Pudasainee, K. Molecular structure, homo-lumo analysis and vibrational spectroscopy of the cancer healing pro-drug temozolomide based on dft calculations. *AIMS Biophys.* **9**, 208–220 (2022).
113. Mondal, S. K., Khan, A. G., Ali, M. M., Ahamed, M. K. & Ahmed, K. Quality of life among Bangladeshi Youth during the early stage of the COVID-19 pandemic: A single-site survey. *Public Heal. Pract.* **2**, 100157 (2021).
114. Quayum, S. T. et al. Exploring the effectiveness of flavone derivatives for treating liver diseases: Utilizing DFT, molecular docking, and molecular dynamics techniques. *MethodsX* **12**, 102537 (2024).
115. Pearson, R. G. Absolute electronegativity and hardness correlated with molecular orbital theory. *Proc. Natl. Acad. Sci.* **83**, 8440–8441 (1986).
116. Poroikov, V. V., Filimonov, D. A., Borodina, Y. V., Lagunin, A. A. & Kos, A. Robustness of biological activity spectra predicting by computer program PASS for noncongeneric sets of chemical compounds. *J. Chem. Inf. Comput. Sci.* **40**, 1349–1355 (2000).
117. Anzali, S. et al. Discriminating between drugs and nondrugs by prediction of activity spectra for substances (PASS). *J. Med. Chem.* **44**, 2432–2437 (2001).
118. Druzhilovskiy, D. S. et al. Computational platform Way2Drug: From the prediction of biological activity to drug repurposing. *Russ. Chem. Bull.* **66**, 1832–1841 (2017).
119. Lagunin, A., Stepanchikova, A., Filimonov, D. & Poroikov, V. PASS: Prediction of activity spectra for biologically active substances. *Bioinformatics* **16**, 747–748 (2000).
120. Talukder, M. E. K. et al. Cheminformatics-based identification of phosphorylated RET tyrosine kinase inhibitors for human cancer. *Front. Chem.* **12**, 1–18 (2024).
121. Goyal, B. & Goyal, D. Targeting the dimerization of the main protease of coronaviruses: A potential broad-spectrum therapeutic Strategy. *ACS Comb. Sci.* **22**, 297–305 (2020).
122. Corvino, A. et al. Phloroglucinol-derived medications are effective in reducing pain and spasms of urinary and biliary tracts: Results of Phase 3 multicentre, open-label, randomized, comparative studies of clinical effectiveness and safety. *Adv. Ther.* **40**, 619–640 (2023).
123. Peron, G. et al. Antiviral and antibacterial properties of phloroglucinols: A review on naturally occurring and (semi)synthetic derivatives with potential therapeutic interest. *Crit. Rev. Biotechnol.* **44**, 319–336 (2024).
124. Chang, Y. T. et al. Anti-EMT and anti-fibrosis effects of protocatechuic aldehyde in renal proximal tubular cells and the unilateral ureteral obstruction animal model. *Pharm. Biol.* **60**, 1198–1206 (2022).
125. Liu, M., Hansen, P. E. & Lin, X. Bromophenols in marine algae and their bioactivities. *Mar. Drugs* **9**, 1273–1292 (2011).
126. Pagare, P. P. et al. The antisickling agent, 5-hydroxymethyl-2-furfural: Other potential pharmacological applications. *Med. Res. Rev.* https://doi.org/10.1002/med.22062 (2024).
127. Li, M. M. et al. The protective role of 5-HMF against hypoxic injury. *Cell Stress Chaperones* **16**, 267 (2010).
128. Erickson, K. L., Beutler, J. A., Gray, G. N., Cardellina, J. H. & Boyd, M. R. Majapolene a, a cytotoxic peroxide, and related sesquiterpenes from the red alga Laurencia majuscula. *J. Nat. Prod.* **58**, 1848–1860 (1995).
129. Li, K., Li, X. M., Gloer, J. B. & Wang, B. G. Isolation, characterization, and antioxidant activity of bromophenols of the marine red alga Rhodomela confervoides. *J. Agric. Food Chem.* **59**, 9916–9921 (2011).

Acknowledgements

We are thankful to the Bioinformatics Laboratory (BioLab), Bangladesh for providing software support, training, and assistance during the work.

Author contributions

Conceptualization NHS; Data curation SMS, MMK, MIH, and NHS; Formal analysis SMS, MMK, MIH, AAR, MNN, and NHS; Investigation MIH, FMP, and NHS; Methodology SMS, MMK, MIH, AAR, MNN, JF, MRA, NK, and NHS; Resources NHS; Software NHS; Writing - original draft SMS, MMK, MIH, AAR, MNN, JF, MRA, NK, and NHS; Supervision NHS; Validation SMS, MMK, MIH, and NHS; Visualization MIH, JF, MRA, NK, and NHS; Writing – review & editing SMS, MMK, MIH, FMP, and NHS; All authors have read and agreed to the submitted/published version of the manuscript.

Funding

The author(s) received no financial support for the research, authorship, and/or publication of this article.

Declarations

Competing interests

The author(s) declared no potential conflicts of interest with respect to the research, authorship, and/or publication of this article.

Ethical statement

This research involves no animal model. So, this is not applicable for this.

Additional information

Supplementary Information The online version contains supplementary material available at https://doi.org/10.1038/s41598-025-15030-8.

Correspondence and requests for materials should be addressed to N.H.S.